USGS
science for a changing world

Helicopter Electromagnetic and Magnetic Survey Data and Maps, Northern Bexar County, Texas

By Bruce D. Smith, Michael J. Cain, Allan K. Clark, David W. Moore, Jason R. Faith, and Patricia L. Hill

Open-File Report 05-1158

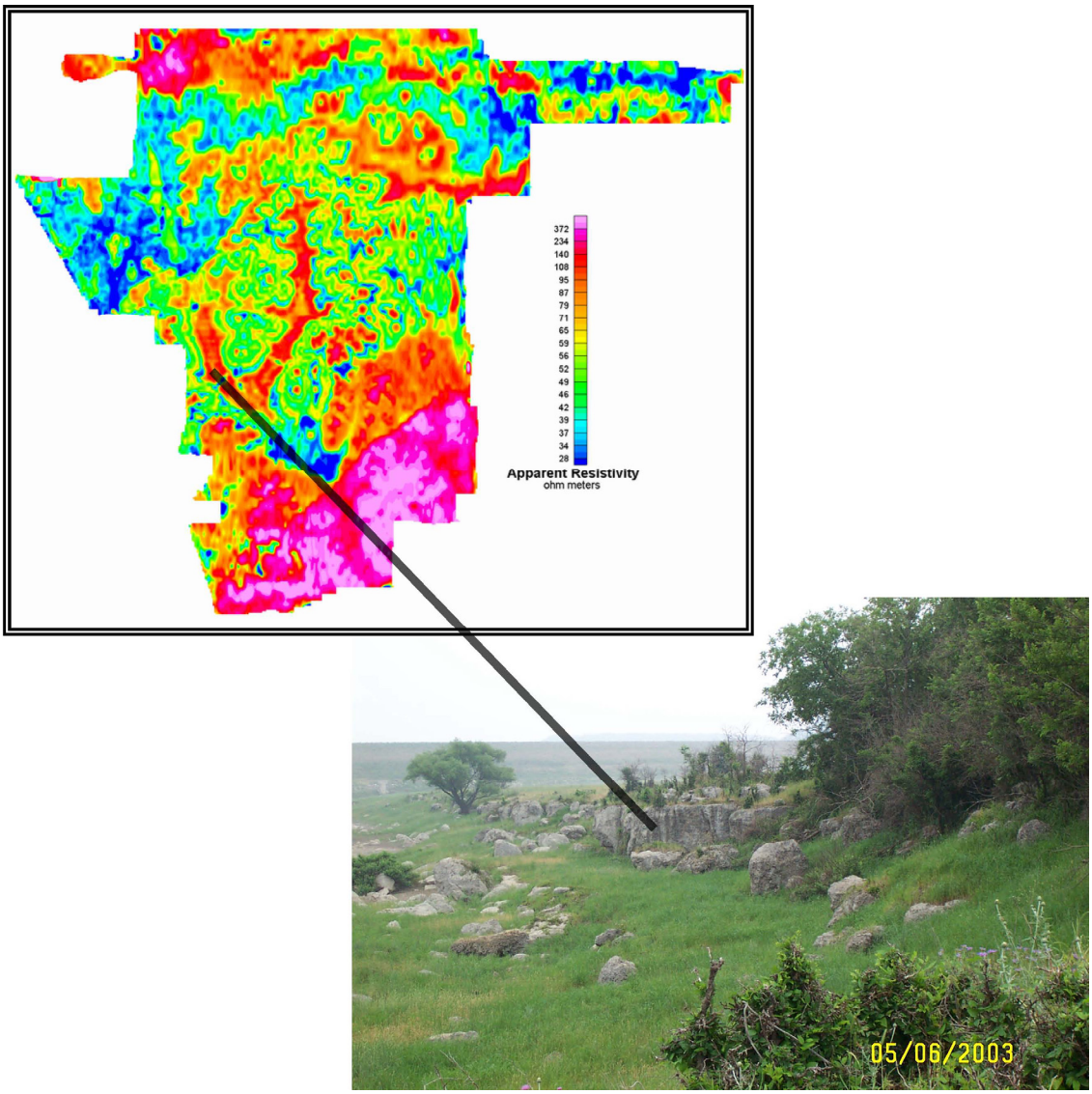

DEPARTMENT OF THE INTERIOR
U.S. GEOLOGICAL SURVEY
In Cooperation with U.S. Army Camp Stanley Storage Activity, U.S. Army Camp Bullis, Edwards Aquifer Authority, San Antonio Water System

Front Cover:
Colored apparent resistivity map at 115,000 Hz with highs shown in warmer colors. Photograph (A.K. Clark, 2003) looking south along Salado Creek at Camp Bullis training site. The outcropping rocks compose a biostrome in the upper Glen Rose Limestone (hydrogeologic unit D). The hill in the background is the earthen dam across Salado Creek. The black line shows approximate location of the biostrome on the geophysical map.

Disclaimer:
Any use of trade, product, or firm names is for descriptive purposes only and does not imply endorsement by the U.S. Government.

U.S. Department of the Interior
Gale A. Norton, Secretary

U.S. Geological Survey
Charles G. Groat, Director

U.S. Geological Survey, Reston, Virginia 2005
Revised and reprinted: 2005

For product and ordering information:
World Wide Web: http://www.usgs.gov/pubprod
Telephone: 1-888-ASK-USGS

For more information on the USGS—the Federal source for science about the Earth,
its natural and living resources, natural hazards, and the environment:
World Wide Web: http://www.usgs.gov
Telephone: 1-888-ASK-USGS

This report has not been reviewed for stratigraphic nomenclature

Although this report is in the public domain, permission must be secured from the individual

copyright owners to reproduce any copyrighted material contained within this report.

Summary

This open-file report is a data release for a helicopter electromagnetic (HEM) and magnetic geophysical survey flown in early December 2003, in Northern Bexar County, Texas (fig. 1). The U.S. Geological Survey (USGS) contracted the survey to Fugro Airborne of Toronto, Canada. Fugro flew a similar survey under contract to the USGS in the Seco Creek area (fig. 1) of the Edwards aquifer (Smith and others, 2003). The objective of these surveys was to collect geophysical data to map and image subsurface features important in understanding ground-water resources in the area (Smith and others, 2003). In particular, the survey has refined the location of mapped faults in the survey area and suggested many unmapped faults exist. These faults can control ground-water flow and storage. New lithologic variations in the Edwards Recharge were mapped in both the shallow and deep subsurface. Images of the subsurface in the confined zone demonstrated a structural complexity not previously appreciated. Geophysical mapping in the Trinity aquifer also showed previously unmapped structures and lithologic variations.

****
Figure 1. General index map showing areas of airborne electromagnetic surveys carried out in Edwards Aquifer studies.
****

The success of the airborne geophysical work at Seco Creek (Smith, Irvine, and others, 2003)". led to a meeting of USGS and Camp Stanley Storage Activity (CSSA, Brian Murphy) personnel organized by Parsons Technology (Gary Cobb) to evaluate the possible use of airborne geophysical methods at that site. The area of the CSSA, about 10 square miles, is considerably smaller than the Seco Creek survey area of 80 square miles. Consequently, the general cost per line mile for this small area was estimated to be a factor of 4 to 5 times higher than for the larger area of the Seco Creek survey. A proposal was submitted to the Camp Bullis environmental group to expand the survey area to include the military training site adjacent to CSSA. The USGS also submitted a funding proposal to the San Antonio Water System (SAWS) to fly the Cibolo Creek area north of the military sites and a proposal to the Edwards Aquifer Authority to fly the Edwards recharge area to the south. All of the proposals, in addition to the CSSA proposal, were at least partly funded. The resulting survey consisted of about 800 line miles (1,280 line kilometers) of HEM flying with a major portion of the area being Camp Bullis.

A major constraint in flying the areas adjacent to the military sites and northern Bexar County is that urbanization of the city of San Antonio is rapidly expanding to the north, thus restricting low-level

flying. An important reason for the project to map and to understand the subsurface Edwards aquifer is that it is the sole-source water supply for the city. As the city development expands northward in Bexar County, less area will be available for low-level aerial surveying including geophysics. A detailed map of survey boundaries is shown in figure 2.

****
Figure 2. Detailed index map of the Northern Bexar County study area with numbered flight lines. Background is digital raster graphics (DRG) topographic image provided as part of this data release.
****

Geophysical Survey Summary

The HEM survey used the RESOLVE© system flown by Fugro Airborne Surveys, which uses five horizontal coplanar coils and one vertical coaxial coil for electromagnetic field measurements. Appendix I, the contractor's report, gives details of the instrumentation and data processing procedures. The specific frequencies for the electromagnetic system are given in table 1. These frequencies are similar to those used in the Seco Creek survey except for the highest frequency that was nominally 100,000 Hz. The geophysical sensor housing ("bird") includes the electromagnetic (EM) system, a total field magnetometer, differential kinematic Global Positioning System (GPS) and laser altimeter. The helicopter carries another differential GPS system, barometric and radar altimeters, and a video camera. Electromagnetic noise from power lines and natural sources (lightning) also are measured. The survey was flown with east-west flight lines and a nominal line spacing of 200 m with a sensor elevation of 30 m except as required for safety considerations and FAA regulations. In-fill lines were flown in the central part of the survey area to yield an effective flight line spacing of 100 m. Lines were also flown down Salado and Lewis Creeks (see cover photo) for additional resolution along drainages. North-south tie lines were flown to level the total field magnetic data.

Table 1. Frequencies and sensitivities for the HEM survey.

Coil Configuration	Nominal Frequency Hertz	Actual Frequency Hertz	Sensitivity parts per million
Coplanar	400	389	0.12
Coplanar	1,500	1,574	0.12
Coaxial	3,300	3,245	0.12
Coplanar	6,200	6,075	0.24
Coplanar	26,000	25,300	0.60
Coplanar	115,000	114,940	0.60

Data-Release Summary

The digital data are described in detail in the following sections and in the contractor report (Appendix I). The data are organized into separate subdirectories in this data release. The subdirectories contain "readme" files describing the files in that directory. Table 2 is a summary of these directories with active links. The geographic data are referenced to NAD27, UTM14N unless otherwise specified. The line data in the "LINEDATA" directory are given in a Geosoft OASIS MONTAJ© database. A free data viewer is available from Geosoft (www.geosoft.com accessed 2/04/05) that can be used to convert the files to ASCII. Files given in the GRIDS subdirectory for the digital magnetic data, apparent resistivity data, and digital terrain model data (derived from the laser altimeter and GPS systems) can be read in the free viewer. Also included is a plug-in (SOFTWARE subdirectory) provided by Geosoft for ESRI programs such as ARCGIS (8.2 and higher) that reads Geosoft grids. The digital maps are all referenced to NAD27, UTM14N.

Table 2 Digital data subdirectories (active hyperlinks) showing type of data and general format.

SUBDIRECTORY	DESCRIPTION	DATA FILE TYPE
REPORTS	reports	Word and PDF
LINEDATA	flight line x,y,z	Geosoft databases
GRIDS	gridded geophysical data	Geosoft grids
FIGURES	figures and plates used in reports	png and pdf
SOFTWARE	plugins for viewing and using data	executable programs
GIS	miscellaneous geographic information system files	various formats
GEOTIFF	geo-referenced bit map images NAD27, UTM14N	tiff and tfw

The airborne geophysical project for northern Bexar County includes an interpretational component. A report on results of this part of the study is in progress. Preliminary comparison of the new geophysical maps with the published geologic maps (A.K. Clark; 2003, 2004) show that the airborne survey provides new information about the location of structures and near surface lithologic variations. The apparent resistivity maps at the 6 survey frequencies provide a rough estimate of conductivity variations as a function of depth. The geophysical data suggest that 1) northwest trending structures that cross the northeast trend of the Balcones fault system are more extensive than currently mapped (A.K. Clark, 2003), 2) apparent resistivity trends in the Edwards recharge zone suggest possible lithologic or structural variations that have not been mapped, 3) the apparent resistivity data from the highest frequency (115,000 Hz) has trends that closely follow the mapped geology and suggest lithologic variations not previously mapped, and 4) differences in the lithologies of the Trinity and Edwards aquifers imply possible constraints in location of subsurface ground water flow paths. All of these preliminary

interpretational observations suggest that further processing of the electromagnetic data will be useful in refinement of subsurface geologic and hydrologic features. Processing which is under way includes screening of areas affected by power line noise, and construction of resistivity depth sections (cross sections of resistivity variations) along each flight line.

GEOLOGIC SETTING

Quaternary and Recent Sediments

A quick survey of surficial geologic deposits was done in February of 2004 to examine whether such deposits were extensive enough in the study area to warrant further mapping. The largest and thickest surficial geologic deposits were found in the valley of Salado Creek in the area of the Camp Bullis firing ranges. Elsewhere in the area of Camp Bullis, only thin alluvium (meter or fractions of a meter) very narrow in aerial extent is present in the valleys. The hilly uplands have very limited surficial material. Residuum or colluvium commonly is not more than several centimeters thick. However, bedrock exposures, mostly limestone, are limited due to this thin surficial material. Conclusions from this field reconnaissance are that surficial geologic deposits are not thick enough to justify further geologic mapping and they have not significantly influenced the high frequency airborne resistivity mapping. A more detailed description of specific areas investigated follows the description of the airborne geophysics.

Bedrock Geology

The Cretaceous sedimentary sequence in the study area consists of the Edwards Group and underlying Glen Rose Limestone that have been described in detail by Rose (1972). The stratigraphic nomenclature for these units is given in table 3. In the study area, the Edwards Group is juxtaposed against the older Upper Glen Rose Limestone by faulting in the Balcones Fault zone. The principal set of these extension faults (faults in rocks along which there has been bed-parallel elongation) generally trends southwest to northeast; a smaller set of cross faults trends southeast to northwest. Generally, the faults are en echelon (in step-like arrangement), high-angle (nearly vertical), normal (hanging wall has moved downward relative to foot wall), with the downthrown blocks typically toward the southeast. This fault morphology generally has resulted in a progression from older lower Glen Rose Limestone, exposed in the northern part of the study area, to younger upper Glen Rose Limestone, and to the youngest Edwards Group exposed in the southern most part of the study area. The study area does not extend to the south

where the Edwards Group is overlain by younger confining formations. Not all faults are associated with topographic relief, particularly if the rocks on both sides of a fault have similar weathering characteristics and the rate of movement was similar to the rate of erosion. Additionally, some topographic differences related to faulting are obscured where the bedrock is covered by alluvium, soils, and or vegetation.

The Glen Rose Limestone comprises (informal) lower and upper members over most of Camp Bullis. The upper Glen Rose Limestone characteristically is thin bedded and composed mostly of soft limestones and marl. The "stair-step," terraced-hill topography that is common in much of Central Texas results largely from differential rates of erosion between alternating beds of relatively resistant limestone and comparatively soft marl in the upper Glen Rose Limestone.

The lower Glen Rose typically is composed of relatively massive, fossiliferous limestone (Whitney, 1952). These reefal rocks interfinger with mudstones. In its area of occurrence just north of Camp Bullis, the lower Glen Rose Limestone is about 320 feet thick (Ashworth, 1983). At Camp Bullis, about 80 feet of lower Glen Rose Limestone is exposed and clearly visible along Cibolo Creek. The lowermost part of the lower Glen Rose in outcrop is a dense, thick-bedded mudstone that, in some places, appears to form mounds. Above this mudstone are thick bioherms or reef like masses of rock composed of the calcareous remains of aquatic organisms, such as the rudistid (a bivalve). These bioherms are greater than 50 feet thick in some places. They are overlain by about 30 feet of thin-to-medium-bedded (mostly) mudstone with some wackestone and packstone.

The three members of the Kainer Formation of the Edwards Group at Camp Bullis (basal nodular, dolomitic, and Kirschberg evaporite) are composed of nodular limestone, mudstone (some places chalky), *miliolid* grainstone, highly altered crystalline limestone, and chert. Although the individual thickness of each member at Camp Bullis is unknown, the cumulative thickness in Bexar County ranges from about 210 to 250 feet (Stein and Ozuna, 1995, table 3).

Table 3. Nomenclature and lithologic units for the stratigraphic sequence in the northern Bexar study area (modified from Clark, A.K., 2003).

Group, formation, member			Thickness (feet)	Lithology
Edwards Group	Kainer Formation	Kirschberg evaporite member	50–60	Highly altered crystalline limestone; chalky mudstone; chert
		Dolomitic member	110–130	Mudstone to grainstone; crystalline limestone; chert
		Basal nodular member	50–60	Shaly, nodular limestone; mudstone and *miliolid* grainstone
Glen Rose Limestone		Upper member	120+	Alternating and interfingering medium-bedded mudstone, wackestone, and packstone with evaporites locally
			120–150	Alternating and interfingering mudstones, marls, wackestone, and packstones
			10–20	Yellow-to-white calcareous mud and vuggy mudstone
			135–180	Thin-bedded mudstone; thin-to-medium-bedded wackestone, packstone, and thick bedded rudist biostromes locally
			10–20	Yellow calcareous mud and vuggy mudstone
		Lower member	320	Thick-bedded mudstone; thin-to-medium-bedded mudstone, wackestone, packstone, and marls
Pearsall Formation		Bexar Shale member	40–70	Dark mudstone, clay, and shale

Hydrogeologic Setting

The hydrogeologic features of the study area (fig. 3) are best related to specific lithologies of each formation that can be related to permeability and porosity characteristics. Stricklin and others (1971) informally subdivided the Glen Rose Limestone into eight lithologic units. Clark (2003, 2004) subdivided the Glen Rose Limestone into five hydrogeologic units as given in figure 3b. These informal subunits, described below, can be related to the observed electrical properties of rocks in the study area. A generalized hydrogeologic map of the survey area is shown in figure 3a.

****

Figure 3a. Hydrogeologic map of study area generalized from Clark, A.K. (2003, 2004) and Clark, A.R. (2003). Blue lines are major drainages, and red lines show major faults.

Figure 3b. Legend for geologic and hydrogeologic map units and lithologic section for outcropping rocks in the northern Bexar County study area.

****

Edwards Group

The Dolomitic and Basal Nodular Members of the Edwards Group form caves and karst and thus are important to the ground-water flow paths in the study area. There are no recognized hydrologic subdivisions for the Edwards Group in the study area beyond the recognized geologic units (table 3).

Glen Rose Limestone Upper Member

Interval A: This interval, about 120 feet thick, has been referred to as the "cavernous zone" (George Veni, George Veni & Associates, written commun., 2000) because of its relatively abundant caves. Veni (written commun., 1998) has mapped the occurrence of caves in the Glen Rose Limestone throughout south-central Texas and has graphically demonstrated a greater density of caves in this interval compared to Interval B. The cave development here is associated with well-developed fracture, channel, and cavern porosity. This not-fabric selective porosity has become interconnected over geologic time and thus permeable enough to now provide avenues for appreciable amounts of water to enter and flow through the subsurface. The contact between the Glen Rose Limestone and overlying Kainer Formation is characterized locally by cavern porosity and extremely high permeability—properties that appear to decrease with depth below land surface.

Interval B: This interval, about 120 to 150 feet thick, is similar to Interval A but with appreciably less cave development and thus less permeability overall than Interval A. The mudstones and marl that compose the major part of this interval have low not-fabric selective porosity and appear to have little, if any, permeability. This interval typically is more of a confining unit than it is an aquifer.

Interval C: About 10 to 20 feet thick, this interval is mostly a remnant of rocks containing relatively soluble carbonate minerals. Interval C is characterized by (fabric selective) breccia porosity, boxwork (intersecting blades or plates) permeability, and collapse structures associated with the dissolution of evaporites. Tending to retard the vertical percolation of ground water, this relatively thin layer diverts much of the water laterally to discharge from contact springs and seeps where the bedding intersects the land surface. Outcrops of this unit are rare and typically obscured as a result of deep weathering.

Interval D: Interval D, about 135 to 180 feet thick, is located between two intervals of partly to mostly dissolved evaporites (Intervals C and E). Owing to an abundance of rudist biostromes and a profusion of *Orbitolina texana*, Interval D is known among geologists as the "fossiliferous zone." Although this interval generally has low porosity and little permeability, there are local exceptions. In a few locations, some cavern porosity can be seen along fractures in the outcrop. The cross-bedded and ripple-marked grainstone marker bed at the top of Interval D has well developed (fabric selective) moldic and (not-fabric selective) vug, channel, and fracture porosity; although thin, the marker bed appears to be permeable. The caprinid biostrome just below the top of Interval D also appears to have excellent (fabric selective) moldic and (not-fabric selective) vug, fracture, and cavern porosity, which probably is sufficiently interconnected to be permeable. Interval D, in addition to containing many of the stock ponds common to northern Bexar County, has numerous springs that discharge from the top along contacts with overlying rocks of partly to mostly dissolved evaporites.

Interval E: As in Interval C, this relatively thin (10 to 20 feet) layer of partly to mostly dissolved evaporites—which includes the *Corbula* bed at its base—appears to divert the downward percolation of ground water laterally toward seeps at land surface. Many of these seeps continue to transmit water even during drought. Like Interval C, this layer likely is characterized by boxwork permeability provided by (fabric selective) breccia porosity that resulted from collapse following the dissolution of evaporites. Although boxwork and collapse structures have not been observed at Camp Bullis (perhaps because weathering effects are obscuring such exposures), they can be observed just west of Camp Bullis.

Glen Rose Limestone Lower Member

At the top of the lower Glen Rose Limestone, the thin-to-medium-bedded mudstone, wackestone, and packstone appear to have low porosity and little permeability with only (not-fabric selective) fracture porosity evident and no cavern development. Field observations indicate that the largest porosity and greatest permeability in the lower Glen Rose Limestone have developed in the rudist bioherms about 10 m below the top of this unit. The rudist zone contains well developed (fabric selective) moldic porosity and (not-fabric selective) fracture and cavern porosity. Large sinkholes and other solution structures have formed in this zone. Downward migration of water appears to be hampered by dense mudstone underlying the rudist zone; the mudstone is the lowermost exposed (along Cibolo Creek) rock of the lower Glen Rose. The only porosity evident in this mudstone appears to be fracture porosity, some of which has been enlarged by dissolution. The effect of the low porosity and little permeability characteristic of this mudstone is demonstrated in the bed of Cibolo Creek where unconnected waterholes contain water even during drought.

Description of Basic Digital Data

The helicopter geophysical survey was conducted in December of 2003. The airborne system consisted of instrumentation both on the helicopter and in a system towed beneath the helicopter as described in detail in Appendix I. Digital recording instrumentation in the helicopter consisted of a differential GPS system, a radar altimeter, and a barometric altimeter. The main part of the geophysical system is towed beneath the helicopter in a 10-m long tube. The electromagnetic measurements are done with a set of six coils operating at different frequencies and coil configurations (table 1). The towed system also contains the total field magnetometer, a laser altimeter, and differential GPS system. The differential GPS utilized a base station located in the northern part of the Camp Stanley Storage Activity (CSSA), which also was the base of operations where a base station magnetometer was located. The contractor's report, Appendix I, gives details of the data instrumentation, acquisition, and processing, and contains the digital line data.

Digital data contained in this report have been organized in subdirectories given in table 2. The basic digital navigation was done using a WGS84 datum and then converted to NAD27 to conform to other USGS Edwards Aquifer projects. The line data given in the LINEDATA subdirectory have x, y, z locations for both coordinate systems. Post-processed maps and gridded data are given in NAD27 UTM14N projection.

The airborne digital acquisition system speed and airborne flight speed result in sampling of data

along flight lines (fig. 2) of about 3 m. Flight lines were flown along Lewis and Salado Creeks for additional detail. Two flight lines were flown on the east and west sides of the survey area for magnetic field measurement leveling. A small area of CSSA, designated B3, was flown with north-south flight lines with 50 m spacing. Results from this area will be discussed in detail in a subsequent report. The entire survey was flown with 200-m spacing and then 100-m in-fill lines were flown in the central area for additional detail (fig. 2).

Considering that the spacing between flight lines is much greater than the spacing of samples along the lines, gridding of the flight data is usually done with cells that are on the order of 1/5 the flight line spacing. Because the survey has areas with both 200-m and 100-m flight line spacing the following procedure was used to make the grids of the digital flight line data. First the area of 100-m flight line spacing was gridded with a cell size of 20-m. The area flown with 200 m spacing was gridded with a cell size of 40-m and then regridded to reduce the cell size to 20-m. The two grids then were merged together with a 40-m overlap. The resulting final grid cell size for the whole survey area was 20-m.

An important part of the interpretation of the airborne geophysical data is based on the digital terrain elevation and digital measurement of the sensor height. The digital terrain model (DTM in the digital data base) is calculated from the helicopter differential GPS system in conjunction with the radar and barometric altimeters. The DTM grid is given in the GRIDS subdirectory (file; dtm_20m). The resolution of the DTM has not been thoroughly evaluated but the GPS systems have a 2 m resolution. The DTM has been checked against the published USGS digital raster graphics 1:24,000 topographic maps for the study area. Major topographic features correlate well. This correlation also is used to cross-check geographic projection of the digital data sets. Figure 4 shows a DTM map of the study area. The geo-referenced tiff image for the map can be found in the GEOTIFF subdirectory.

****
Figure 4. Map of the digital terrain model (DTM) for the northern Bexar County HEM study area. Heavy black lines indicate boundaries of the military sites, and the blue lines show the major drainages.
****

The subdirectory GIS contains several digital files which have been used in the figures for this report. Geo-referencing for these files is NAD 27 UTM14N. The digital raster graphics (DRG) maps for the topographic sheets in the study area have been converted to a compressed format using the Earth Resources Mapping (ERMAPPER, 2004) compression software. The parts of the topographic quadrangles that are in the HEM study area is shown in the images. The compressed maps are files

bexar_hem_drg_nocolor.ecw (no green vegetation color) and bexar_hem_drg.ecw in the directory (GIS). Other files in the GIS subdirectory are described in table 4.

Table 4. Description of files located in the GIS digital data subdirectory.

FILE NAME	DESCRIPTION
bullis_boundary.dxf	Boundary of Camp Bullis
cssa_fenceline_27cor.dxf	Boundary of CSSA
flight_path.dxf	flight path for HEM survey
NBexarGeoNad27.tfw	world file for location of hydrogeologic map
nbexargeonad27.tif	generalized hydrogeologic map
streams_nad27_edit.dxf	main drainages for study area
survey_area_boundary.dxf	bounding box for HEM survey

Airborne Magnetic Field Data

Magnetic Method

The magnetic system (magnetometer described in Appendix I) measured the earth's total field to an accuracy of 0.01 nanotesla (nT). The magnetic field consists of the earth's main magnetic field and of the local magnetic field due to both sources within the crust and to ferromagnetic metallic sources at the surface.

In general, the bedrock in the survey area is non-magnetic. The only highly magnetic rocks in the Trinity-Edwards Aquifers are younger intrusive rocks that occur to the west of San Antonio (Smith and Pratt, 2003). No intrusive rocks are known or expected to occur in this study area. Consequently, small high magnetic anomalies are mostly due to metallic cultural features. Very small linear magnetic features

could be associated with alteration along some faults, such as a small magnetic low associated with the Woodard Cave fault in the Seco Creek survey area (Smith and Pratt, 2003). Processing of the total magnetic field maps to emphasize these small magnetic features may enhance possible magnetic signature of faults.

Magnetic Field Data

The contractor's report in Appendix I describes processing of the magnetic field measurements in detail and this information is not repeated here. The resulting total magnetic field intensity (TMI) has been corrected for the international geomagnetic reference field (IGRF) trend. The TMI grid is given as file TMI.GRD in directory GRIDS\Mag_Girds. All of the preprocessing magnetic field data are given in the digital database in subdirectory LINEDATA. Two additional processing steps have been applied to these magnetic field data. The first step is to reduce the main magnetic field to the pole, which shifts magnetic highs to be located directly over the causative body instead of being shifted slightly to the south. Figure 5a shows the reduced-to-the-pole (RTP) magnetic field for the study area. The grid for the reduced-to-the-pole (RTP) magnetic data is file mag_rtp.grd in the GRIDS\Mag_Grids subdirectory (Table 2. A geo-referenced tiff file, mag_rtp.tiff is located in the GEOTIFF subdirectory. The second step is to remove a regional magnetic field. This was accomplished by fitting a third order polynomial surface to the RTP magnetic data using Oasis Montaj software (Geosoft, Inc., 2004). This surface then was subtracted from the RTP map to produce the residual map (fig. 5b). File mag_rtp.grid is given in the GRIDS\Mag_Grids subdirectory and a geo-referenced tiff file; mag_residual.tiff is given in the GEOTIFF subdirectory.

****
Figure 5. Total magnetic field maps for the northern Bexar County HEM study area a) reduced to the pole (RTP) magnetics b) Residual magnetic field with third order regional magnetic field removed.
****

Airborne Electromagnetic Data

Electromagnetic Method

In general the rock units in the study area consist of centimeter to hundreds of meter thick layers of limestones and mudstones that are interlayered. The following electrical properties were interpreted from the Seco Creek airborne survey (Smith, Irvine, and others, 2003). The massive limestones of the

Edwards Group are generally associated with high resistivities in the hundreds of ohm-meters. In contrast, mudstones of the Glen Rose Formation have resistivities ranging from less than 10 to more than 50 ohm-meters. The highly altered collapsed evaporite units are moderately to highly conductive (1 to 50 ohm-meters).

The RESOLVE© helicopter electromagnetic (HEM) system flown by Fugro Airborne consists of six coil pairs with frequencies given in table 1. The electromagnetic measurements at different frequencies are much like a medical "CAT" scan of the earth (see a good lay discussion by Won, 1990) in that they can be used to image the subsurface electrical properties of rocks. For example in the human body, bones have different electrical properties than tissue and appear as light areas in CAT scans. In much the same way, the processed images of the earth discussed here have red areas that indicate high resistivities such as limestones or other electrically resistive rocks. CAT scans are accomplished by moving the electromagnetic system around the patient to produce a three-dimensional image or "tomogram." The HEM method is limited, of course, in that it can only be moved above the surface of the earth. The subsurface images of the earth are less resolved than CAT scans because of this and other limitations.

One important consideration of the HEM earth subsurface imaging is that the depth of imaging is dependent on the frequency and resistivity of the earth. One estimate of the depth of exploration (depth of mapping) for the frequencies used in the RESOLVE© system is shown in figure 6. In this figure, the depth of exploration is defined as 0.5 of the skin depth (point at which a plane electromagnetic wave has attenuated to 37 per cent of the initial amplitude). The depths of exploration estimates shown in figure 6 are conservative since one skin depth generally is considered to be the depth limit of HEM measurements (Fraser, 1978). Generally, at the highest frequency, depths of exploration are just a few meters. At the lowest frequency, 400 Hz, the depth of exploration may be on the order of 80-m. This aspect of HEM resistivity measurements is the basic principle that allows depth images to be constructed.

****
Figure 6. Depth of penetration or imaging as a function of frequency and earth resistivity for the RESOLVE© system (Hodges, Fugro Airborne, 2004, written communication).
****

Power Line Monitor

The airborne electromagnetic system also monitors 60 Hz signals in coaxial (CXPL channel) and coplanar (CPPL channel) coil configurations given in the line database (LINEDATA). The data are given as arbitrary voltage levels, which generally increase over power lines. The grid for the coplanar configuration (coplanar_powerline.grd) is given in the GRIDS subdirectory. Figure 7 shows the map of the power line monitor variations for the study area in arbitrary voltage units. The geo-referenced tiff image for the map can be found in the GEOTIFF subdirectory as file coplanar_powerline.tiff. The expression of power lines in the map (fig. 7) is quite variable due to a number of factors such as the size of the line, how well it is "grounded", and the electrical resistivity of the earth. In general the infrastructure around the urban development as well as development on the military sites creates a higher cultural noise level in the northern Bexar study area than in the Seco Creek study survey (Smith, Irvine, and others, 2003).

****

Figure 7. Map of the power-line monitor from the coplanar coil pair for the northern Bexar County HEM study area. Heavy black lines indicate boundaries of the military sites and the blue lines show the major drainages. Highs shown in the warmer colors generally are due to power-line sources. No color scale is given since units are in arbitrary voltages.

****

Scattered small anomalies in the central power line 60 Hz map (fig. 7) indicate the coupling of radiated signals to the geophysical electromagnetic system. Interestingly, the high 60 Hz noise in the system resulted in higher noise in the apparent resistivity maps for the northern Bexar HEM survey than for the earlier Seco survey. Figure 8 shows part of the apparent resistivity data along a flight line in each survey area. Several filtering methods were experimented with to reduce this noise in the apparent resistivity maps. For the lowest frequency (400 Hz), the normal 11-point Hanning filter expanded to 13 points was sufficient to remove the high frequency noise in the grids. A broad filter of this sort normally is not used in mineral exploration HEM surveys because a main objective is find small sharp anomalies at lower frequencies. Filtering of the HEM data is discussed in Appendix I.

****

Figure 8. Flight line plots from a) Seco Creek survey and b) northern Bexar survey. Data shows the effects of noise along the flight lines. The filter applied along the flight line is described in the text. The high pass residual is the result of subtracting the measured from the filtered data.

****

Apparent Resistivity Maps

Apparent resistivity is the resistivity of a homogeneous isotropic volume that would give the same electromagnetic signal as measured by the HEM system. Fugro Airborne, as part of the contracted data processing, computed the apparent resistivity for each frequency. The computation is based on the pseudo-layer model (Fraser, 1978). Figure 9 and plate 1 show apparent resistivity maps for the six frequencies (table 1) measured by the RESOLVE© system. Note that the apparent resistivity map for 3,300 Hz has been placed at the bottom of the map sequence (high to low frequency) to emphasize that the coaxial coil configuration differs from the horizontal coil configuration for the other five frequencies. The coaxial coil system is more sensitive to power lines and vertical electrical inhomogeneities than are the coplanar coil pairs.

****

Figure 9. Apparent resistivity maps of the northern Bexar County HEM study area for the nominal frequencies of the survey system: (a) 115,000 Hz, (b) 25,000 Hz, (c) 6,400 Hz, (d) 400 Hz, (e)1,500 Hz, and (f) 3,300 Hz. Plate 1 shows larger maps and color scales.

****

The color scale has the same stretch between the highest and lowest measured apparent resistivity for each map (frequency). The highest apparent resistivity decreases 1.5 orders of magnitude as frequency decreases (see figure caption), from 1,300 to 150 ohm-meters. The color scales have been used to emphasize comparative high and low resistivity areas within each map (at each frequency) rather than between maps. A color scale is used where high resistivity (low conductivity) areas are in the warmer colors (reds) and areas of low resistivity (high conductivity) in the cooler colors (blues). Using the same high to low color stretch for each map emphasizes trends and linear features but does not emphasize that the average apparent resistivity decreases as a function of decreasing frequency.

In general, each map in figure 9 shows progressively deeper sections (from fig. 9a to 9e) of the earth. Also, the volume of the subsurface that is sampled increases as a frequency decreases. Consequently, the resolution of electrical features decreases with depth. The effects of power line noise also increases as a function of decreasing frequency. Examination of the lower frequency apparent resistivity maps (fig. 8 and Pl. 1) in comparison to the power-line monitor map (fig. 7) shows that most of the power lines produce linear areas of low resistivity (blues). In contrast, the highest frequency (115 kHz) appears to be little affected by the power lines. However, note that due to the shallow penetration

depth at this frequency, it also will show resistivity responses from man-made structures such as the earthen dams across Salado and Lewis Creeks.

In-fill lines were flown for the central part of the survey area in order to increase the mapping resolution. Figure 10 shows a comparison of the added detail gained from the in-fill flying. The narrow small "worm-like" high resistivity zones that follow the trends of Lewis and Salado Creek are the surface and near-surface expression of limestone units in the Edwards hydrogeologic interval B. The major trends correlate well with the hydrogeology as mapped by Clark, A.R. (2003). The in-fill flying was critical in defining the interlayered mudstones and limestones, which are shown in finer detail in the airborne geophysics than in the more general hydrogeologic map (Clark, A.K., 2003).

****
Figure 10. Comparison of apparent resistivity maps at 115,000 Hz for 200 m and 100 m spaced flight lines. Color scale is the same as shown in plate 1 where the warmer colors are higher resistivity. Blue lines are Salado (west) and Lewis (east) Creeks.
****

Grids located in the GRIDS subdirectory are described in Table 5 below. Generally, the apparent resistivity grids are named with the prefix RES followed by the nominal frequency such as RES1500.GRD. The file format is in Geosoft OASIS MONTAJ (Geosoft, 2004).

Table 5. Description of subdirectories in the GRIDS subdirectory.

GRIDS Subdirectory	
DIRECTORY (CAPS) OR FILE NAME	**DESCRIPTION**
GRIDS_ALL	Resistivity and magnetic field grids all of the flight lines except area B3.
GRIDS_B3	Resistivity and magnetic field grids for B3
MAG_GRIDS	Processed total magnetic field includes reduced to the pole (rtp) and residual
RES_GRIDS_FILT	Resistivity grids filtered to remove 60 Hz noise
coplanar_powerline_20m.grd	Power line grid for coplanar configuration (with header file)
dtm_20m.grd	Digital terrain model 20 meter grid (with header file)

Quaternary Investigation

One of the more striking features of the apparent resistivity map at the highest frequency (115,000 Hz; fig. 9; pl. 1) is the high resistivity that follows much of the Salado and Lewis drainages. A field reconnaissance of three areas on Camp Bullis was made on February 24 and 25, 2004, to assess the influence, if any, of Quaternary and recent sediments on the results of the HEM survey. The following describes observations for the areas visited.

Area 1–Salado Creek valley

Clayey gravelly alluvium underlies the broad terrace from Bullis Road southeast to Wilderness Road. The alluvium is granules, pebbles, cobbles, and minor boulders in a 20–30 percent clay matrix. This unit is estimated to be 5–15 ft thick, as much as 20 feet locally, and consists of limestone clasts with no quartz or feldspar. It probably is water saturated in rainy seasons. The 5 to 10 foot-wide Salado Creek

channel bottoms out on limestone bedding planes; locally, thin piles of boulders rest in the channel. Capping the alluvium (on broad terrace, see map) is sticky, plastic wet clay soil about 1 to 1.5 feet thick.

From the earth dam upstream to Cowgill Road, massive limestone 6 ft thick is covered discontinuously by black, sticky, plastic clay, 0 to 8 inches thick; slightly pebbly. The map extent of this description closely matches the pattern of red color depicted on the 115,000 Hz apparent resistivity map. The earthen dam across Salado Creek (cover photograph) is associated with a low resistivity (blue area, fig. 10) that likely is due to the clay material of the dam.

Detailed observation–site A: Reservoir upstream from large earth dam on Salado Creek, 100-m west of Marne Road. Surficial material is brownish-black (5 YR 2/1) sticky, plastic clay, 3 to 12 inches thick that discontinuously overlies massive limestone bed. Exposed in the stream-bed is a medium gray massive limestone bed (3 to 5 ft thick) that has a horizontal to 1 degree south dip, vuggy Swiss cheese–like texture owing to dissolution, scarce caverns, and small cave(s). This same unit is dense (not vuggy) in other places farther north in valley. This lithology is exposed across the 400-m wide valley north of the earthen dam. Over several areas, up to an acre or two in size, a single bare, horizontal limestone bedding plane crops out. On the hillsides on the west and east sides of the valley, gullies and bulldozed roads expose thin, alternating beds of nodular, marly limestone, nodular limestone, a few dense, massive limestone beds, and yellow, calcareous mudstone. Brecciated carbonate minerals in these exposures are suggestive of evaporite dissolution more than 100 ft thick. These units overlie the massive limestone in the valley, forming stripes and "bulls-eye" outcrop patterns on nearby domal hills. Generally, the reservoir area in Salado Creek has a thin plastic clay that discontinuously veneers a massive, thick, dense to vuggy limestone, stripped to a bare bedding plane in many places.

Detailed observation–site B: This area is located upland east of Salado Valley 0.5 mi east of Cowgill and Marne Roads intersection. It is characterized by patches of sticky clay soil 6 inches deep, alternating with bare limestone horizontal bedding planes; abundant pieces of loose limestone cover parts of the surface, and very little soil but much exposed rock. Footslopes along Marne road have a thin layer (0–6 inches) of sheetwashed and colluvial clay and small pieces of limestone abundantly scattered on surface. Level land west of Marne Road (at east edge, Salado Creek Valley), sheetwashed clay from hillslopes above and pieces of limestone, pebbles, and cobbles.

Detailed observation–site C: Salado Creek flat valley floor at Cowgill and Monterrey Roads (at bridge across Salado Creek on Cowgill Road). Flat valley floor about 400 m across, underlain by about

4 ft thick clayey, sandy, granule and pebble to cobble limestone gravel. Well exposed in cutbank. Bedding distinct, planar bedding. One or two interbeds 2 inches thick of clay. Channel is floored with 1–2 ft thick tabular limestone cobbles and boulders. Channel also bottoms on scoured, flat limestone bedding plane in places. Surface soil on floor of valley is 2–8 inches thick, sticky, plastic clay soil containing abundant limestone pebbles and granules.

Area 2: Lewis Creek valley

The area has less than a foot of stony clay over 0–2 ft of clayey limestone gravel, over thick, massive limestone bedrock. A 15–30 ft thick, cliff-forming massive limestone, separated by a few thin marl beds, is widely exposed (bare) in and within 100 m of the entrenched Lewis Creek. Low and thin alluvial terrace deposits are located near the south end of Lewis Creek. There are no recent surficial deposits thick enough to influence airborne resistivity measurements.

Area 3: South of Cibolo Creek

Mostly bare bedrock is in this area, except for one relatively narrow accumulation of sandy gravelly alluvium, 4–8 ft thick. Soils are very thin, spotty, or absent altogether. Where the soil is present (about 20–30 percent of land surface), it is discontinuous, black, sticky, plastic, clay 1–6 inches thick. It is spotty on thin interbeds of clayey, yellowish mudstone and marl. Massive reefal limestone, somewhat gypsiferous, is located in extreme NW corner of Camp Bullis study area (see also lithohydrologic map, Clark, A.K., 2003).

On the 6,200 Hz apparent resistivity plot (fig. 9c, pl. 1c), the distinct, scalloped contact (essentially a line of yellow color) between the rich red color along Cibolo Creek (north edge of map) and the green and blue area of the hills south of it corresponds exactly to the contact between the lower member of the Glen Rose Limestone (the red) and the lowest part of the upper member of the Glen Rose (deep blue on resistivity plot, pl. 1c). This is hydrogeologic unit E (Clark, A.K., 2003), a thin evaporite unit.

The areas of deep blue (pl. 1c) match those areas underlain by alternating thin beds of marl and mudstone, which are clay-rich and possibly gypsiferous units. These units were wet and plastic where probed at the surface. The purple color north of Cibolo Creek in the extreme northwest corner of Camp Bullis is coincident with outcrops of massive, rudistid-reef limestone beds exposed there.

Local alluvium is present along a minor tributary in the watershed. It does not correlate with a signature on the resistivity maps. We speculate that this lack of a resistivity signature reflects a relatively dry alluvium at the time the HEM was flown.

From the above field observations, Quaternary and more recent deposits do not significantly influence the airborne high frequency and thus do not need to be mapped in any additional detail for geophysical interpretation.

Discussion

Apparent resistivity variations reflect changes in bedrock lithologies and can be correlated with hydrogeologic units. A very preliminary association between resistivity and hydrogeologic units is given in table 6. Specific electrical properties are a function of scale. For example, individual thin limestone units may be electrically resistive on the scale of centimeters. On the same scale, mudstones generally should be much less resistive. Intercalation of limestones and mudstones on the scale of tens of meters will have an aggregate electrical signature that is a combination of the individual lithologic units.

In general, the trend of apparent resistivity highs in the upper Glen Rose limestone unit B follows the mapped contacts of Clark (2004). However, at the highest frequency, high apparent resistivity areas indicate more limestone units than mapped by Clark (2004) within this unit. This refinement of the distribution of limestone units is important to an understanding of possible recharge and ultimately to an understanding of possible ground-water flow paths.

The lower Glen Rose limestone exposed along Cibolo Creek has bioherms and reefal units that are surrounded by mudstone units. The limestones are very resistive and probably extend to the south at depth under the CSSA.

Discontinuous trends and linear features in the apparent resistivity maps can be associated with possible structures. The geophysical apparent resistivity mapping suggests greater detail than in the geologic and hydrogeologic mapping of the study area.

Additional work includes compilation of existing electrical and lithologic logs in the study area. New induction conductivity logging for selected drill holes will provide electrical property information for rocks in the unsaturated zone above the water table. Resistivity depth sections will be computed for the electromagnetic data. New structural maps will be interpreted based on the resistivity depth sections.

Depth section maps will be made to show the interpreted resistivity at set depth below the surface or at constant elevation above sea level.

Table 6. Preliminary generalized electrical properties of hydrogeologic units (modified from A.K. Clark, 2003) derived from airborne resistivity measurements. Table 3 describes lithology.

Group, formation, member			Hydrogeologic subdivision			Generalized Resistivity
Edwards Group	Kainer Formation	Kirschberg evaporite member	Edwards aquifer		VI1	Probably low (not exposed in survey area)
		Dolomitic member			VII1	Very high resistivity
		Basal nodular member			VIII1	Very high resistivity
Glen Rose Limestone		Upper member	Trinity aquifer	Upper zone	Interval A	Moderately high resistivity
					Interval B	Moderate to low resistivity
					Interval C	Low resistivity
					Interval D	High resistivity (exposures in Salado and Lewis Creeks field checked)
					Interval E	Very low resistivity (exposures south of Cibolo Creek field checked)
		Lower member		Not subdivided		Bioherms and reefal units have very high resistivity; mudstones low resistivity

References

Ashworth, J.B., 1983, Ground-water availability of the Lower Cretaceous formations in the Hill Country of south-central Texas: Texas Department of Water Resources Report 273, 173 p.

Barker, R.A., and Ardis, A.F., 1996, Hydrogeologic framework of the Edwards-Trinity aquifer system, west-central Texas: U.S. Geological Survey Professional Paper 1421–B, 61 p.

Clark, A.K., 2004, Geologic Framework and Hydrogeologic Characteristics of the Glen Rose Limestone, Camp Stanley Storage Activity, Bexar County, Texas, U.S. Geological Survey, Scientific Investigations Map 2831.

Clark, A.K., 2003 Geologic Framework and Hydrogeologic Features of the Glen Rose Limestone, Camp Bullis Training Site, Bexar County, Texas, U.S. Geological Survey, Water-Resources Investigations Report 03-4081, 9 p.

Clark, A.R., 2003, Vulnerability of ground water to contamination, Northern Bexar County, Texas, U.S. Geological Survey, Water Resources Investigations Report 03-4072, 17 p., 1 pl.

Earth Resources Mapping, 2004, Applications support manual for ECW format, available www.ermapper.com (accessed January 2005).

Fraser, D.C., 1978, Resistivity Mapping with an Airborne Multicoil Electromagnetic System: Geophysics, v. 43, p. 144-172.

Geosoft Inc., 2004, Oasis Montaj Users Manual Version 6, available www.geosoft.com (accessed January 2005), 180 p.

Rose, P.R., 1972, Edwards Group, surface and subsurface, central Texas: Austin, University of Texas, Bureau of Economic Geology Report of Investigations 74, 198 p.

Smith, D.V. and Pratt, D., 2003, Advanced processing and interpretation of the high resolution aeromagnetic survey data over the central Edwards Aquifer, Texas: Proceedings for the Symposium on the Application of Geophysics to Environmental and Engineering Problems, San Antonio, Texas, 14 p.

Smith, B.D., Irvine, R., Blome, C.D., Clark, A.K., and Smith, D.V., 2003, Preliminary Results, Helicopter Electromagnetic and Magnetic Survey of the Seco Creek Area, Medina and Uvalde Counties, Texas: Proceedings for the Symposium on the Application of Geophysics to Environmental and Engineering Problems, San Antonio, Texas, 15 p.

Smith, B.D., Smith, D.V., Hill, P.L., and Labson, V.F., 2003, Helicopter electromagnetic and magnetic survey data and maps, Seco Creek Area, Medina and Uvalde counties, Texas: U.S. Geological Survey Open-File Report 03-226, 43p.

Stein, W.G., and Ozuna, G.B., 1995, Geologic framework and hydrogeologic characteristics of the Edwards aquifer recharge zone, Bexar County, Texas: U.S. Geological Survey Water-Resources Investigations Report 95–4030, 8 p.

Stricklin, F.L., Jr., Smith, C.I., and Lozo, F.E., 1971, Stratigraphy of Lower Cretaceous Trinity deposits

of Central Texas: Austin, University of Texas, Bureau of Economic Geology Report of Investigations 71, 63 p.

Whitney, M.I., 1952, Some zone marker fossils of the Glen Rose Formation of Central Texas: Journal of Paleontology, v. 26, no. 1, p. 65–73.

Won, I.J., 1990, Diagnosing the Earth; Ground-water monitoring review, Summer 1990, National Ground Water Association, 2p.

FIGURES

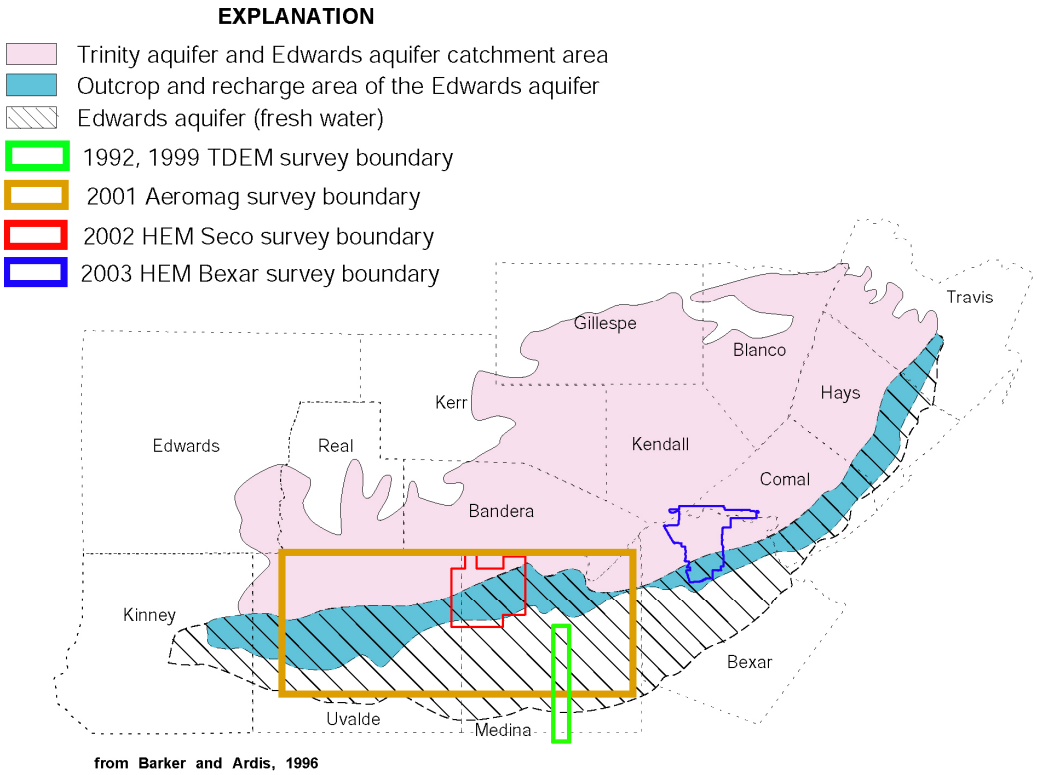

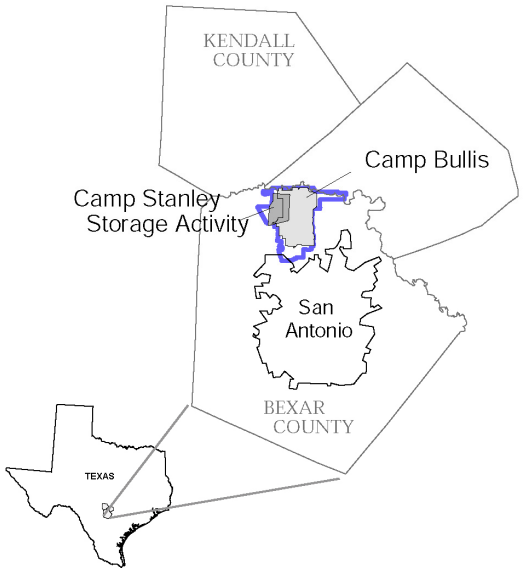

Figure 1. General index map showing areas of airborne electromagnetic surveys carried out in U.S. Geological Survey Edwards Aquifer studies. (return to text page)

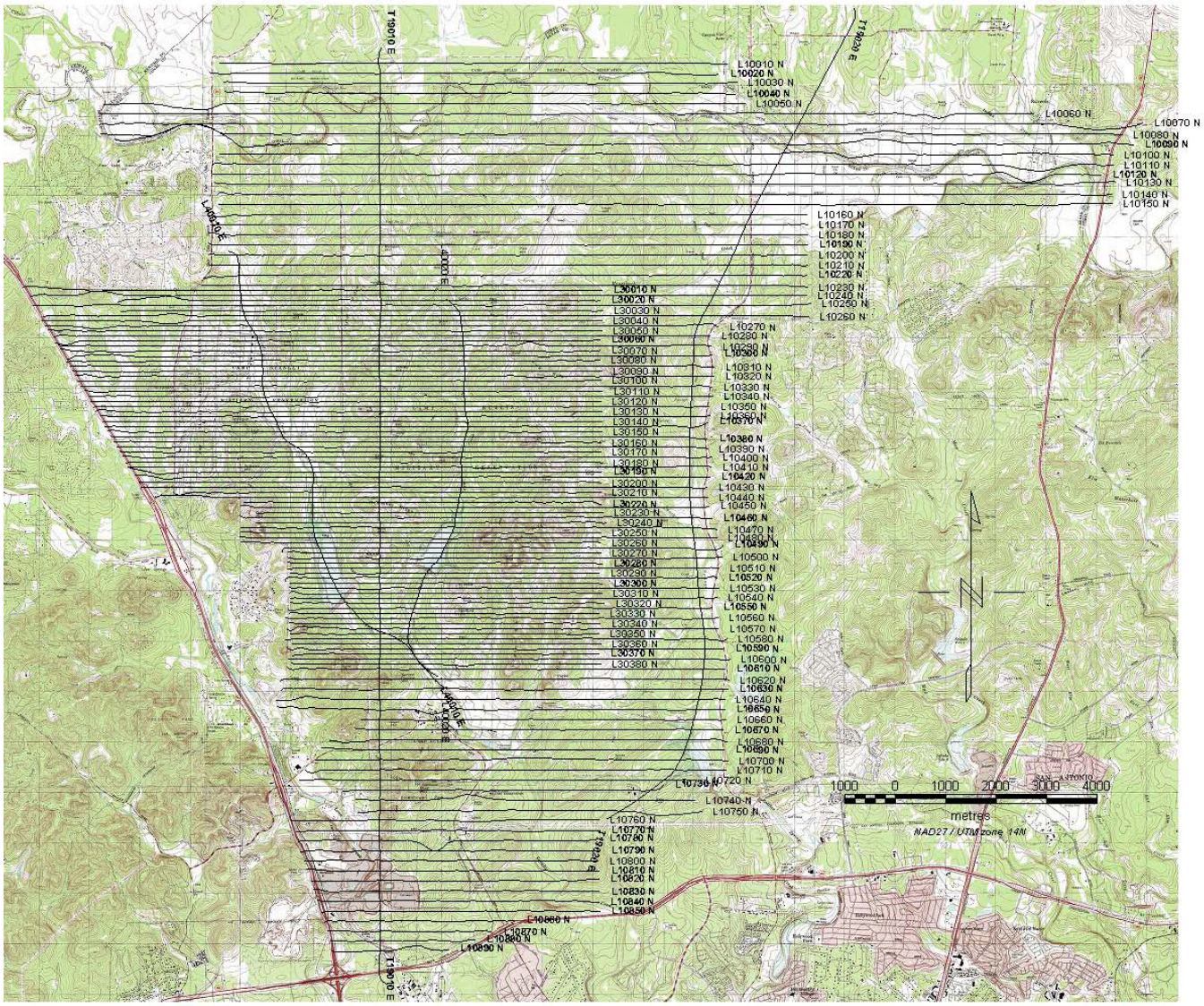

Figure 2. Detailed index map of northern Bexar County with numbered flight lines. Background is digital raster graphics (DRG) topographic image provided as part of this data release. (return to text page)

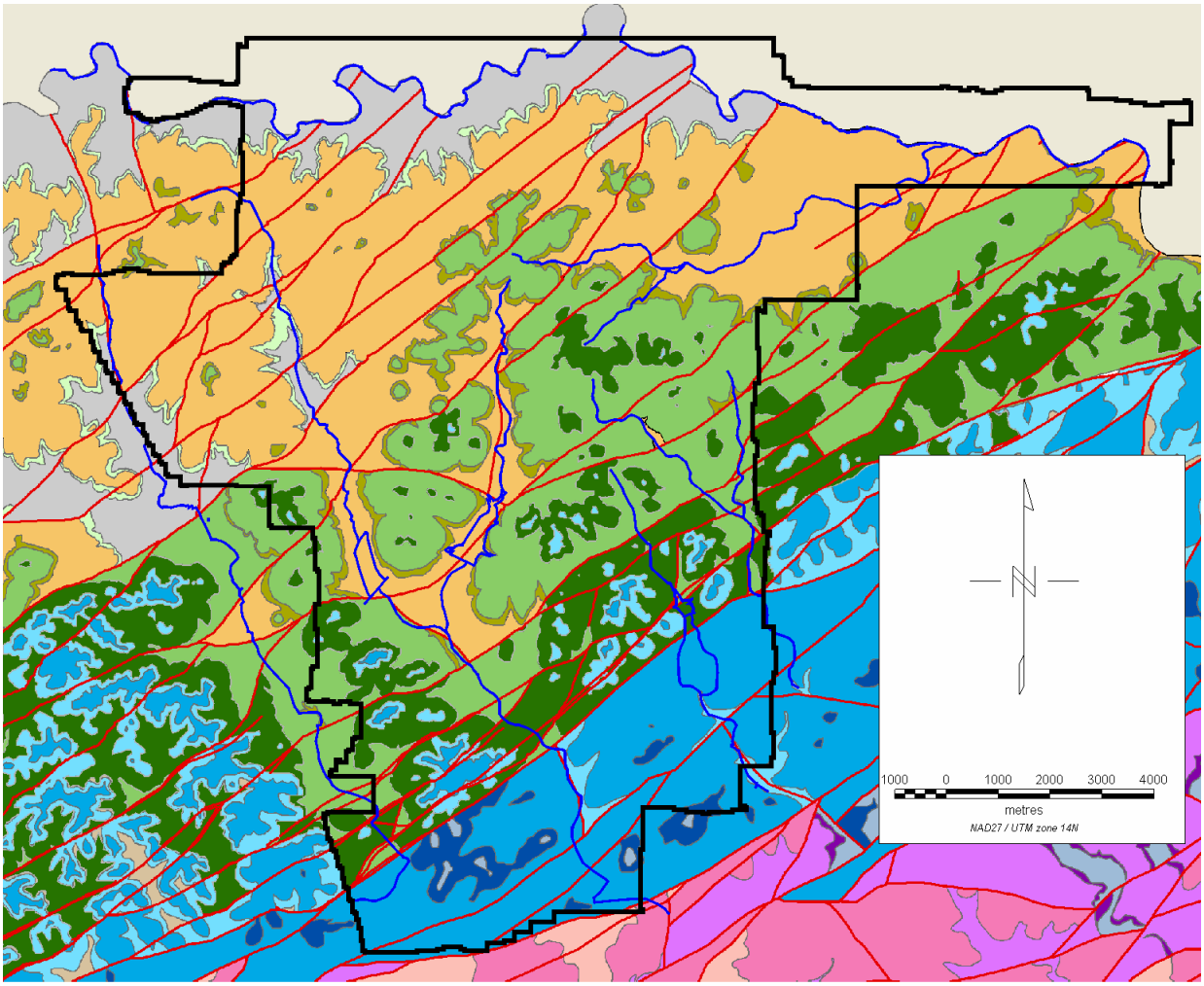

Figure 3a. Hydrogeologic map of the northern Bexar County study area generalized from. Clark, A.K (2003, 2004) and Clark, A.R. (2003). (return to text page)

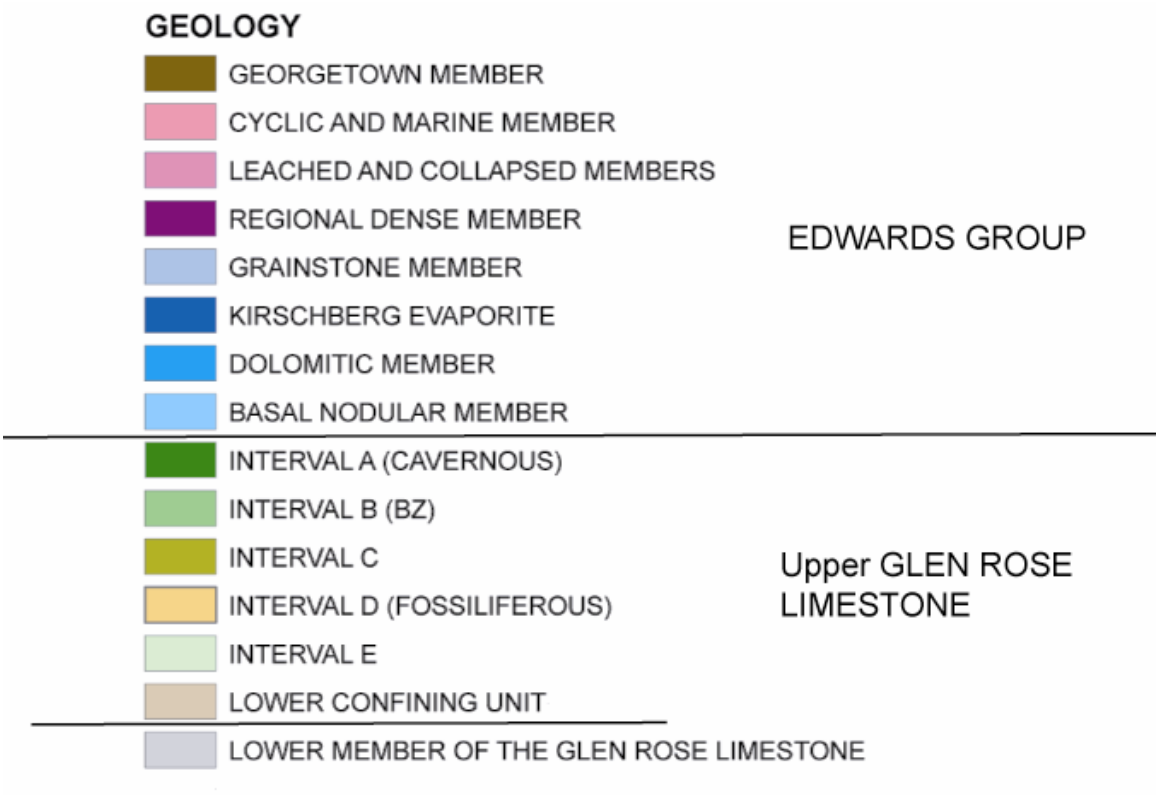

Figure 3b. Legend for geologic and hydrogeologic map units and lithologic section for outcropping rocks in the northern Bexar County study area. (return to text page)

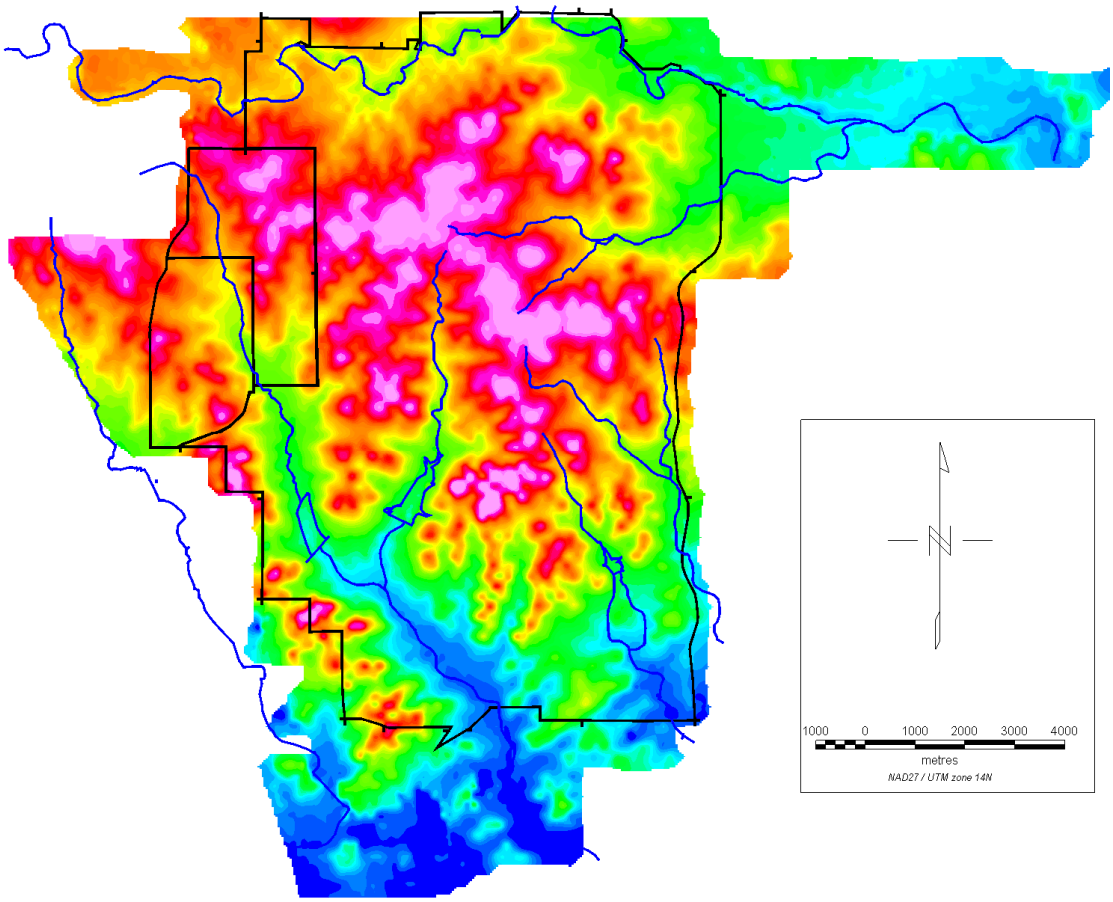

Figure 4. Map of the digital terrain model (DTM) for the northern Bexar County HEM study area. Heavy black lines indicate boundaries of the military sites, and the blue lines show the major drainages.
(return to text page)

a)

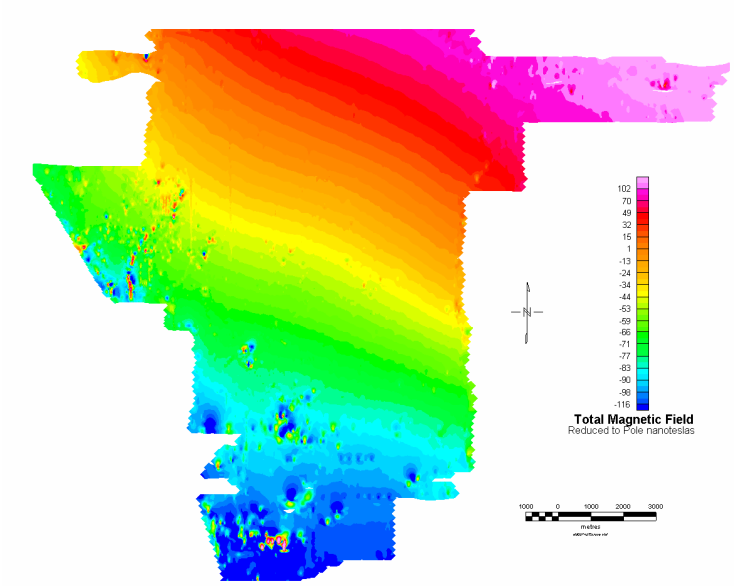

b)

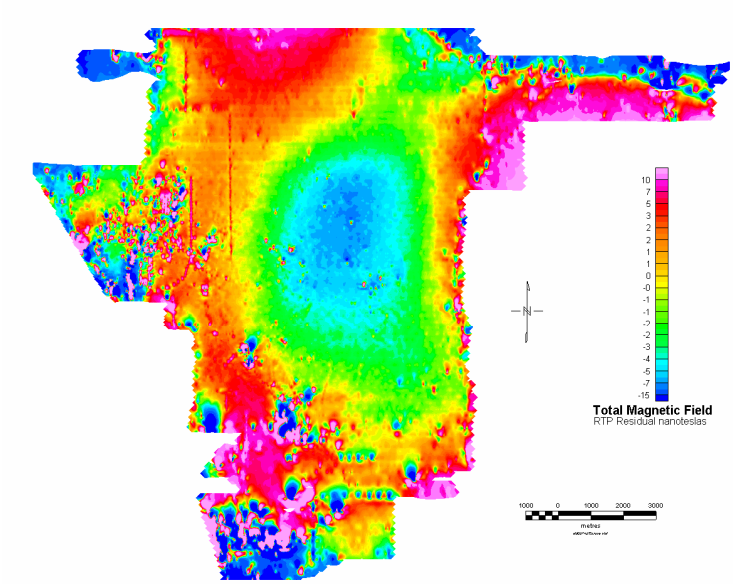

Figure 5. Total magnetic field maps for the northern Bexar County HEM study area: (a) reduced to the pole (RTP) magnetics and (b) Residual magnetic field with third order regional magnetic field removed.
(return to text page)

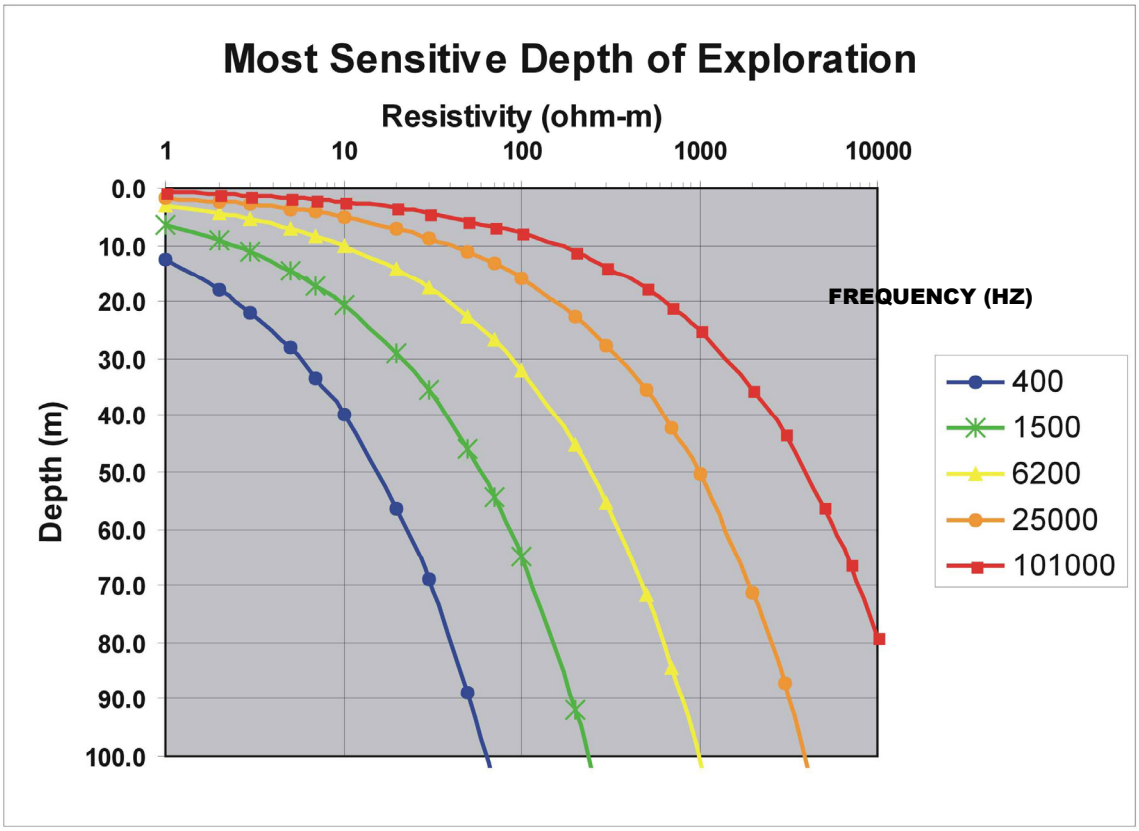

Figure 6. Estimated depth of penetration or imaging as a function of frequency and earth resistivity for the RESOLVE© system (Hodges, 2004, Fugro Airborne, written comm.). (return to text page)

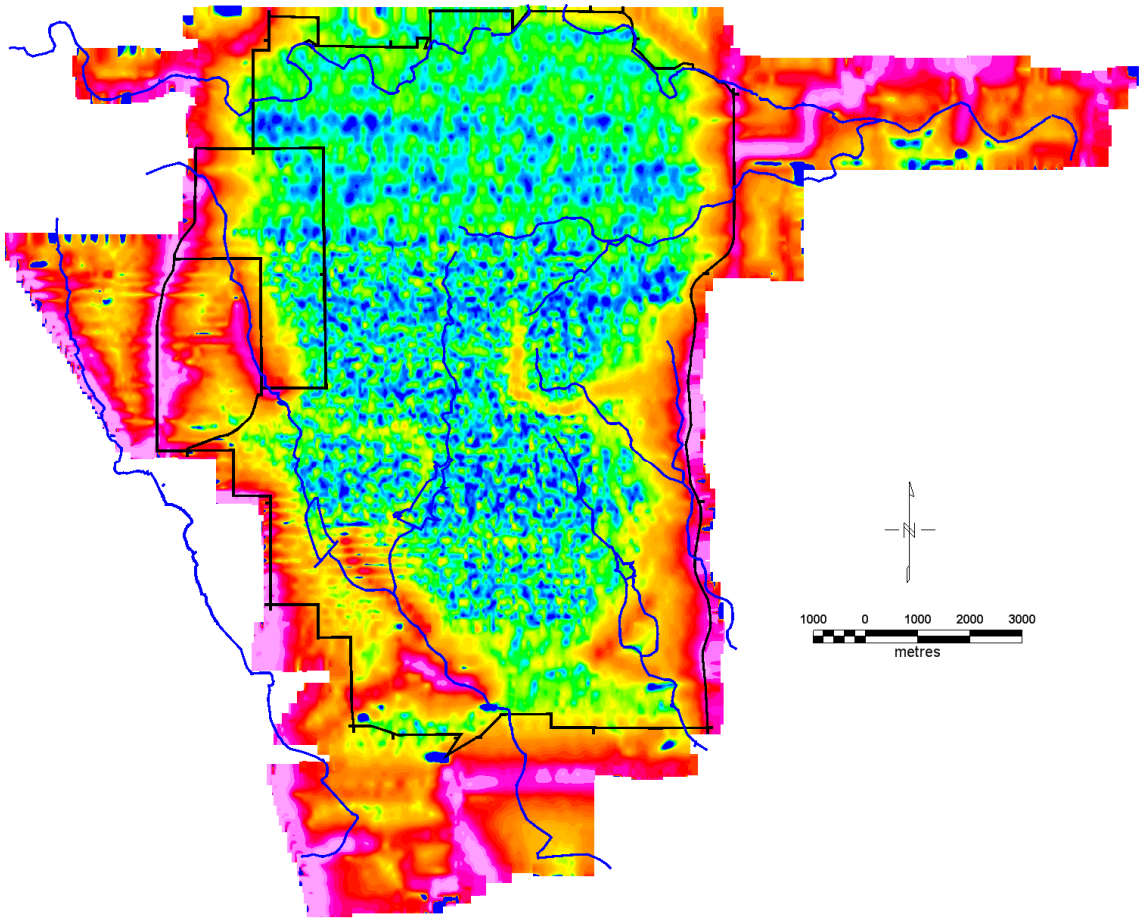

Figure 7. Map of the power-line monitor from the coplanar coil pair for the northern Bexar County HEM study area. Heavy black lines indicate boundaries of the military sites, and the blue lines show the major drainages. Highs shown in the warmer colors generally are due to power line sources. No color scale is given because measurement units are in arbitrary voltages. (return to text page)

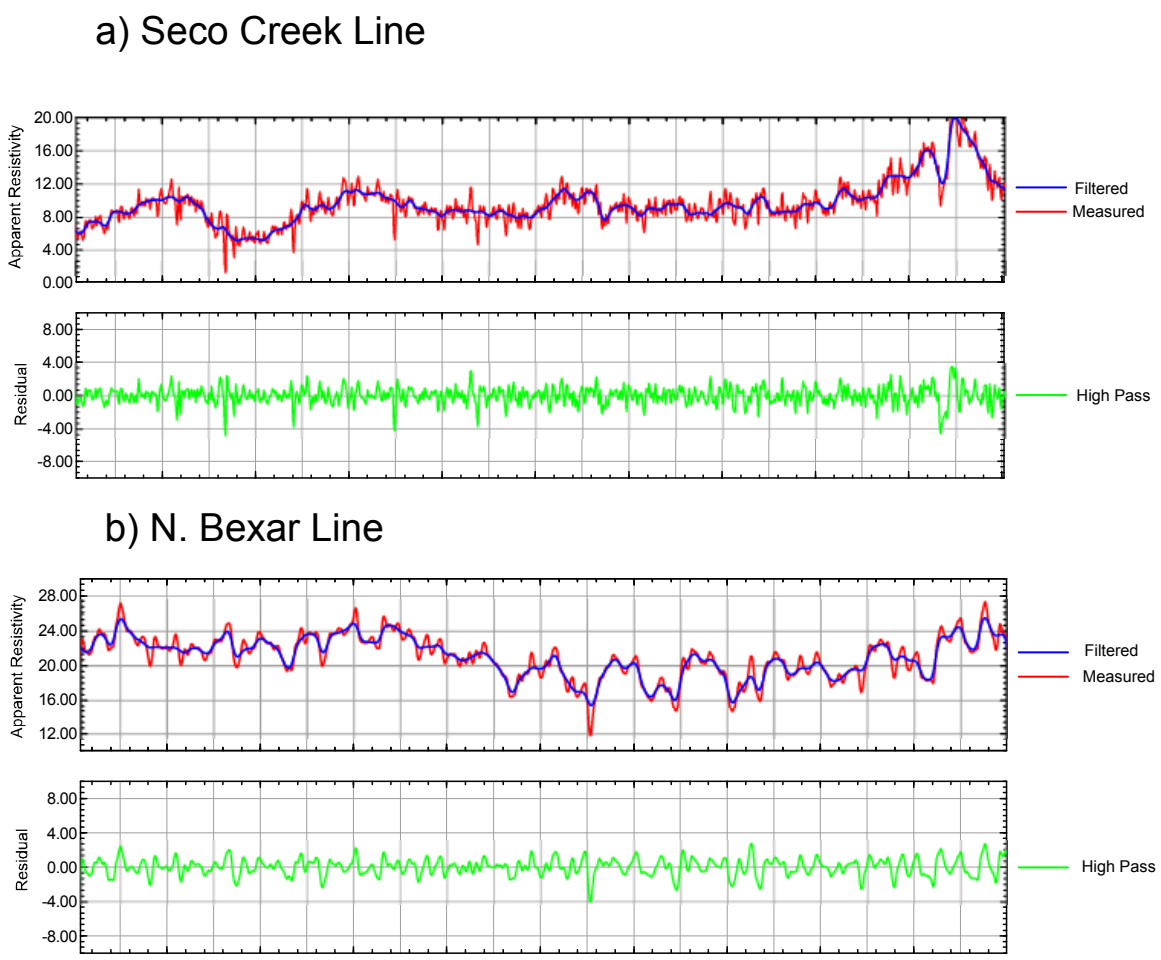

Figure 8. Flight line plots from (a) Seco Creek survey and (b) northern Bexar survey. Data shows the effects of noise along the flight lines. The filter applied along the flight line is described in the text. The high pass residual is the result of subtracting the measured from the filtered data. (return to text page)

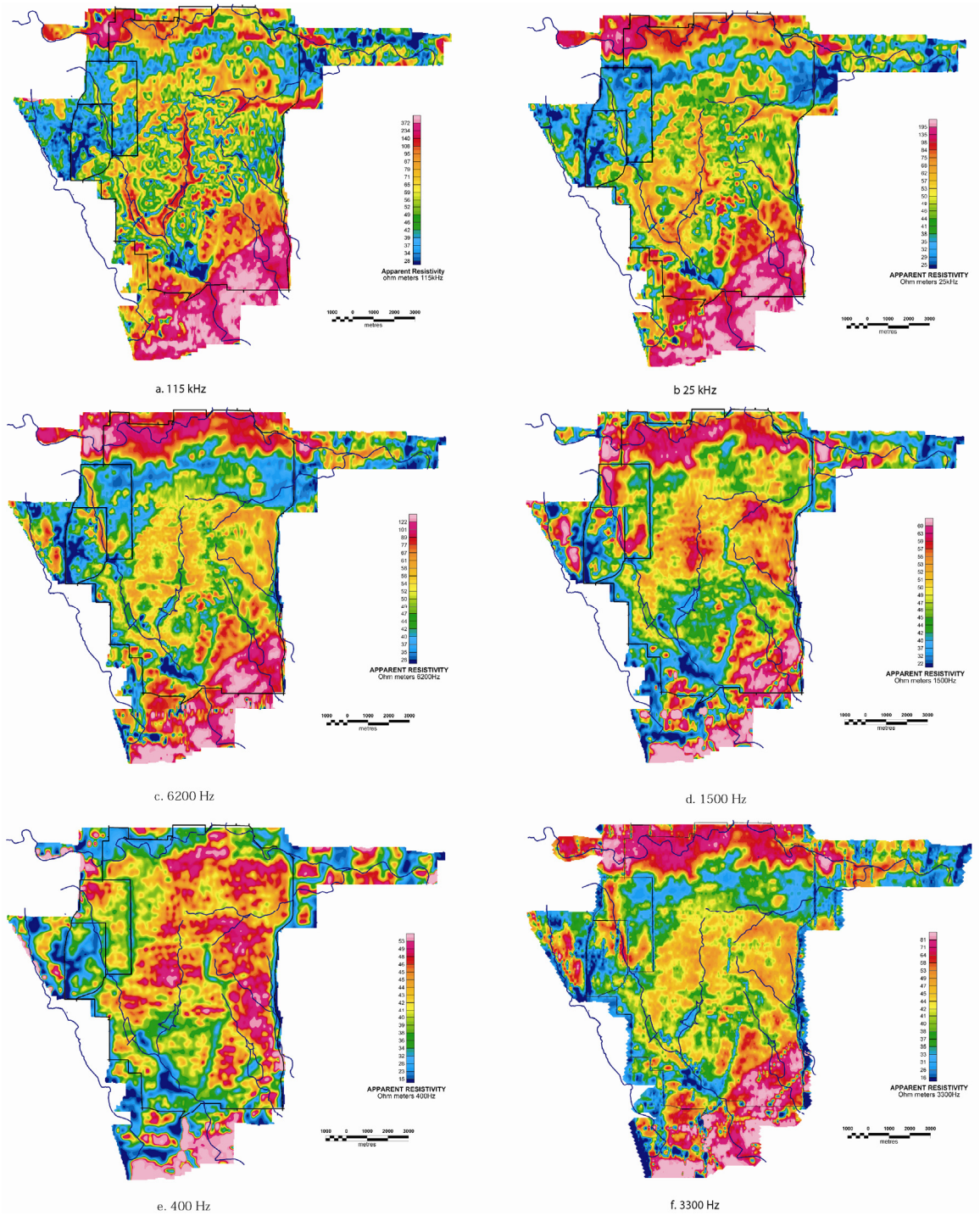

Figure 9. Apparent resistivity maps of the northern Bexar County HEM study area for the nominal frequencies of the survey system: (a) 115,000 Hz, (b) 25,000 Hz, (c) 6,400 Hz, (d) 400 Hz, (e)1,500 Hz, and (f) 3,300 Hz. Plate 1 shows larger maps and color scales. (return to text page)

a)

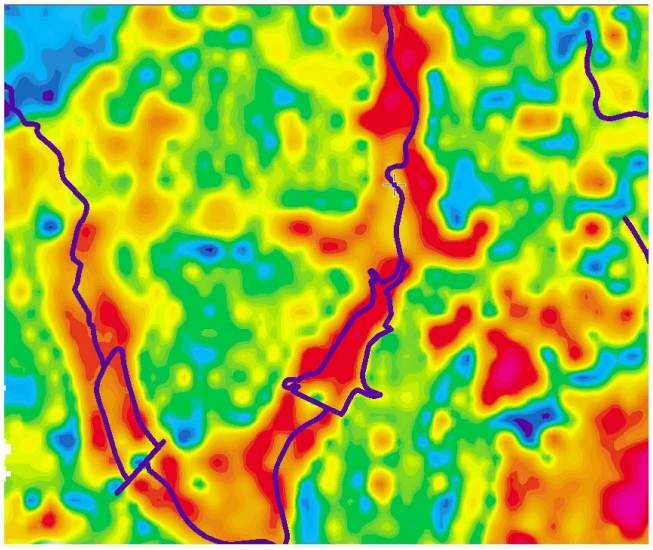

b)

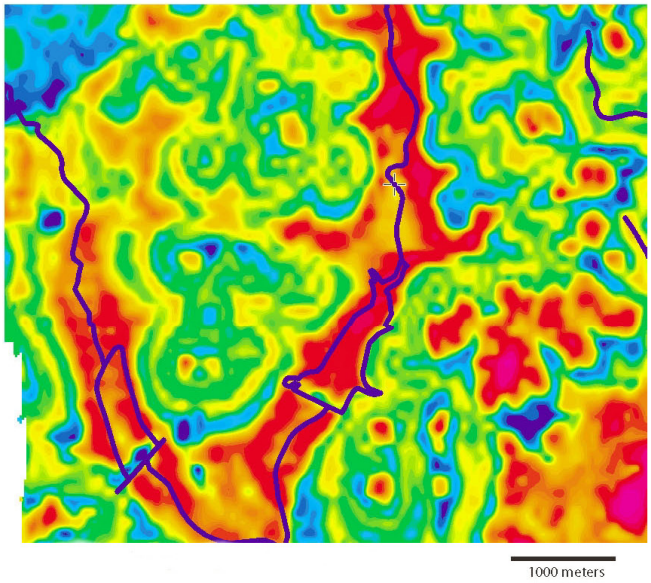

Figure 10. Comparison of apparent resistivity maps at 115,000 Hz for 200 m (a)and 100 m (b) flight lines. Color scale is the same as shown in Plate 1 where the warmer colors are higher resistivity. Blue lines are Salado (west) and Lewis (east) Creeks. (return to text page)

APPENDIX I

Fugro Airborne Report #03069

RESOLVE SURVEY

FOR

U. S. GEOLOGICAL SURVEY

NORTHERN BEXAR COUNTY, TEXAS

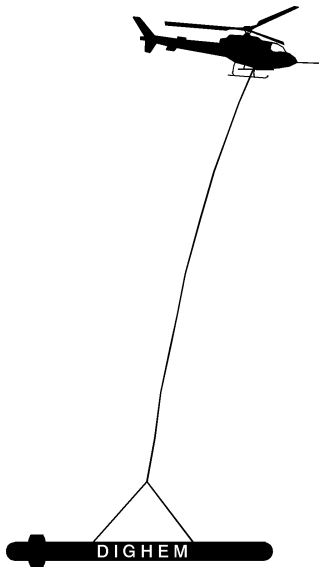

Fugro Airborne Surveys Corp.
Mississauga, Ontario

Michael J. Cain
Geophysicist

March 2004

SUMMARY

This report describes the logistics, data acquisition and processing of a RESOLVE airborne geophysical survey carried out for the U. S. Geological Survey, over parts of northern Bexar County, Texas. Total coverage of the survey blocks amounted to 1281 km. The survey was flown on December 10th to December 14th, 2003.

The purpose of the survey was to map the conductive and magnetic properties of Northern Bexar County in the area of the Edwards Aquifer recharge zone. This was accomplished by using a RESOLVE multi-coil, multi-frequency electromagnetic system, supplemented by a high sensitivity cesium magnetometer. The information from these sensors was processed to produce maps that display the magnetic and conductive properties of the survey area. A GPS electronic navigation system ensured accurate positioning of the geophysical data with respect to the base maps.

The survey data were processed and compiled in the Fugro Airborne Surveys Toronto office. Map products and digital data were provided in accordance with the scales and formats specified in the Survey Agreement.

CONTENTS

APPENDICES

A. List of Personnel
B. Data Archive Description
C. Background Information
D. Flight Logs
E. Tests and Calibrations
F. Processing Log
G. Glossary

1. INTRODUCTION

A RESOLVE electromagnetic/resistivity/magnetic survey was flown for the U. S. Geological Survey from December 10th to 14th, 2003, over part of the Edwards Aquifer recharge zone in Northern Bexar County, Texas.

Survey coverage consisted of 1281 line-km, over 1 block, including a central detail area. A single line was flown along Salado Creek and Lewis Creek within the survey area. Flight lines were flown in an azimuthal direction of 90° with a line separation of 200 metres. The detail area was flown within the main survey area with an offset of 100 metres, giving an effective line spacing of 100 metres within the detail area. Several tie lines were flown perpendicular to the survey lines, but due to flight and schedule restrictions set by the military bases, tie line coverage was limited and not complete in all areas.

The survey employed the RESOLVE electromagnetic system. Ancillary equipment consisted of a high sensitivity cesium magnetometer, radar, laser and barometric altimeters, video camera, analog and digital recorders, and an electronic navigation system. The instrumentation was installed in an AS350-B2 turbine helicopter (Registration C-GZTA) that was provided by Questral Helicopters Ltd. The helicopter flew at an average airspeed of 135 km/h with an EM sensor height of approximately 35 metres.

Figure 1: Fugro Airborne Surveys RESOLVE EM bird with AS350-B3

2. SURVEY OPERATIONS

The base of operations for the survey was established in north San Antonio, Texas. The helicopter was based and fueled out of the San Antonio International airport at Hallmark Aviation. The bird and base stations were located on Camp Stanley. The survey was flown from December 10th – 14th, 2003.

Table 2.1 - Survey Specifications

Parameter	Specifications
Traverse line direction	90°/270°
Traverse line spacing	200 m
Tie line direction	approximately 0°/180°
Tie line spacing	variable
Sample interval	10 Hz or 3.8 m at 135 km/hr
Aircraft mean terrain clearance	62 m
EM sensor mean terrain clearance	35 m
Mag sensor mean terrain clearance	35 m
Average speed	135 km/hr
Navigation (guidance)	±5 m, Real-time GPS
Post-survey flight path	±2 m, Differential GPS

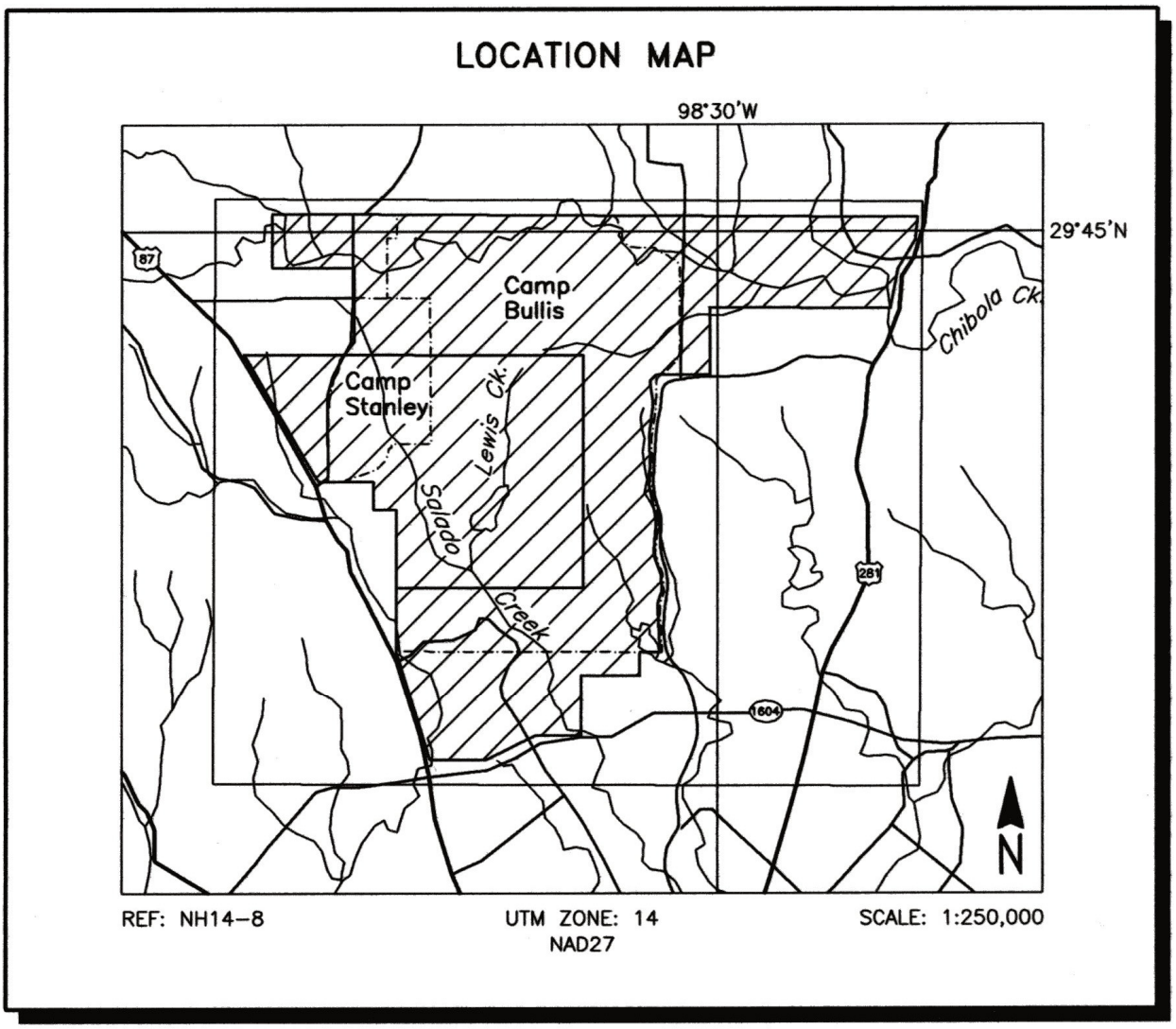

Figure 2

Location Map and Sheet Layout

Northern Bexar County, Texas

Job # 03069

Table 2.2 – Survey Block Corners

Nad27 Utm Zone 14

Block	Corners	X-UTM (E)	Y-UTM (N)
03069-1	1	554854	3291502
Camp Bullis	2	554775	3290742
Camp Stanley	3	554225	3289838
	4	553989	3288514
	5	548092	3288540
	6	548092	3288527
	7	548118	3286340
	8	546362	3286326
	9	546152	3286130
	10	546270	3285422
	11	546144	3284314
	12	546193	3283356
	13	546108	3282944
	14	546387	3281600
	15	546302	3280484
	16	546544	3279853
	17	546593	3279320
	18	546447	3278871
	19	546544	3277333
	20	545881	3277331
	21	545881	3276578
	22	543973	3276578
	23	543973	3274592
	24	542480	3274592
	25	540888	3273797
	26	539067	3273797
	27	537932	3277331
	28	537935	3281908
	29	537203	3281908
	30	537199	3282828
	31	535368	3282828
	32	532939	3286950
	33	536213	3286950
	34	536540	3287382
	35	536531	3289774
	36	533853	3289774
	37	533853	3291523

Nad27 Utm Zone 14

Block	Corners	X-UTM (E)	Y-UTM (N)
03069-3	1	544000	3279400
Camp Bullis	2	537930	3279400
Infills	3	537935	3281908
	4	537203	3281908
	5	537199	3282828
	6	535368	3282828
	7	532939	3286950
	8	544000	3286950
03069-5	1	537199	3287491
B3 Infills	2	537499	3287491
	3	537499	3285491
	4	537199	3285491

3. SURVEY EQUIPMENT

This section provides a brief description of the geophysical instruments used to acquire the survey data and the calibration procedures employed. The geophysical equipment was installed in an AS350-B2 helicopter. This aircraft provides a safe and efficient platform for surveys of this type.

Electromagnetic System

Model: RESOLVE

Type: Towed bird, symmetric dipole configuration operated at a nominal survey altitude of 30 metres. Coil separation is 7.9 metres for 400 Hz, 1500 Hz, 6400 Hz, 25,000 Hz and 115,000 Hz coplanar coil-pairs; and 9.0 metres for the 3300 Hz coaxial coil-pair. The EM bird is towed on a cable measuring 28.7 metres (94 feet). Due to airlift and wind resistance on the bird and cable during flight, a slightly shorter value of 27.7 metres (91 feet) is subtracted from the radar altimeter data to give the approximate bird height. These results agree with the laser altimeter values at survey height and speed.

Coil orientations/frequencies:

orientation	nominal	actual
coplanar	400 Hz	389 Hz
coplanar	1500 Hz1574 Hz	
coaxial	3300 Hz	3245 Hz
coplanar	6400 Hz6075 Hz	
coplanar	25,000 Hz25,300 Hz	
coplanar	115,000 Hz114,940 Hz	

Channels recorded: 6 in-phase channels
6 quadrature channels
2 monitor channels

Sensitivity:	0.12 ppm at 400 Hz CP 0.12 ppm at 1500 Hz CP 0.12 ppm at 3300 Hz CX 0.24 ppm at 6400 Hz CP 0.60 ppm at 25,000 Hz CP 0.60 ppm at 115,000 Hz CP
Sample rate:	10 per second, equivalent to 1 sample every 3.8 m, at a survey speed of 135 km/h.

The electromagnetic system utilizes a multi-coil coaxial/coplanar technique to energize conductors in different directions. The coaxial coils are vertical with their axes in the flight direction. The coplanar coils are horizontal. The secondary fields are sensed simultaneously by means of receiver coils that are maximum coupled to their respective transmitter coils. The system yields an in-phase and a quadrature channel from each transmitter-receiver coil-pair.

RESOLVE System Calibration

Calibration of the system during the survey uses the Fugro AutoCal automatic, internal calibration process. At the beginning and end of each flight, and at intervals during the flight, the system is flown up to high altitude to remove it from any "ground effect" (response from the earth). Any remaining signal from the receiver coils (base level) is measured as the zero level, and removed from the data collected until the time of the next calibration. Following the zero level setting, internal calibration coils, for which the response phase and amplitude have been determined at the factory, are automatically triggered – one for each frequency. The on-time of the coils is sufficient to determine an accurate response through any ambient noise. The receiver response to each calibration coil "event" is compared to the expected response (from the factory calibration) for both phase angle and amplitude, and the applied phase and gain corrections are adjusted to bring the data to the correct value. In addition, the output of the transmitter coils are continuously monitored during the survey, and the applied gains adjusted to correct for any change in transmitter output.

Because the internal calibration coils are calibrated at the factory (on a resistive halfspace) ground calibrations using external calibration coils on-site are not necessary for system calibration. A check calibration may be carried out on-site to ensure all systems are working correctly. All system calibrations will be carried out in the air, at sufficient altitude that there will be no measurable response from the ground.

The internal calibration coils are rigidly positioned and mounted in the system relative to the transmitter and receiver coils. In addition, when the internal calibration coils are calibrated at the factory, a rigid jig is employed to ensure accurate response from the external coils.

Using real time Fast Fourier Transforms and the calibration procedures outlined above, the data will be processed in real time from measured total field at a high sampling rate to in-phase and quadrature values at 10 samples per second.

Airborne Magnetometer

Model:	Fugro AM102 processor with Scintrex CS2 sensor
Type:	Optically pumped cesium vapour
Sensitivity:	0.01 nT
Sample rate:	10 per second

The magnetometer sensor is located inside the EM bird.

Magnetic Base Station

Primary

Model:	Fugro CF1 base station with timing provided by integrated GPS	
Sensor type:	Geometrics G822	
Counter specifications:	Accuracy:	±0.1 nT
	Resolution:	0.01 nT
	Sample rate	1 Hz
GPS specifications:	Model:	Marconi Allstar
	Type:	Code and carrier tracking of L1 band, 12-channel, C/A code at 1575.42 MHz
	Sensitivity:	-90 dBm, 1.0 second update
	Accuracy:	Manufacturer's stated accuracy for differential corrected GPS is 2 metres

Environmental

Monitor specifications: Temperature:

- Accuracy: ±1.5ºC max
- Resolution: 0.0305ºC
- Sample rate: 1 Hz
- Range: -40ºC to +75ºC

Barometric pressure:

- Model: Motorola MPXA4115A
- Accuracy: ±3.0º kPa max (-20ºC to 105ºC temp. ranges)
- Resolution: 0.013 kPa
- Sample rate: 1 Hz
- Range: 55 kPa to 108 kPa

Backup Magnetometer

Model: GEM Systems GSM-19T

Type: Digital recording proton precession

Sensitivity: 0.10 nT

Sample rate: 3 second intervals

A digital recorder is operated in conjunction with the base station magnetometer to record the diurnal variations of the earth's magnetic field. The clock of the base station is synchronized with that of the airborne system, using GPS time, to permit subsequent removal of diurnal drift. The CF1 base station was located at approximately WGS84 LAT 29.7155° and LON 98.6148° at 369.5 metres above the ellipsoid.

Navigation (Global Positioning System)

Airborne Receiver for Real-time Navigation & Guidance

Model:	Ashtech Glonass GG24 with PNAV 2100 interface
Type:	SPS (L1 band), 24-channel, C/A code at 1575.42 MHz, S code at 0.5625 MHz, Real-time differential.
Sensitivity:	-132 dBm, 0.5 second update
Accuracy:	Manufacturer's stated accuracy is better than 5 metres real-time

The antenna for the GPS guidance system is mounted on the tail fin of the helicopter.

Airborne Receiver for Flight Path Recovery

Model:	Ashtech Dual Frequency Z-Surveyor
Type:	Code and carrier tracking of L1 band, 12-channel, dual frequency C/A code at 1575.2 MHz, and L2 P-code 1227 MHz
Sensitivity:	0.5 second update
Accuracy:	Manufacturer's stated accuracy for differential corrected GPS is better than 1 metre

The antenna for the GPS flight path recovery system is housed on the rear of the EM bird.

Primary Base Station for Post-Survey Differential Correction

Model:	Novatel Millennium
Type:	Code and carrier tracking of L1-C/A code at 1575.42 MHz and L2-P code at 1227.0 MHz. Dual frequency, 24-channel
Sample rate:	1.0 second update
Accuracy:	Better than 1 metre in differential mode

Secondary GPS Base Station

Model:	Marconi Allstar OEM, CMT-1200
Type:	Code and carrier tracking of L1 band, 12-channel, C/A code at 1575.42 MHz
Sensitivity:	-90 dBm, 1.0 second update
Accuracy:	Manufacturer's stated accuracy for differential corrected GPS is 2 metres.

The Ashtech GG24 is a line of sight, satellite navigation system that utilizes time-coded signals from at least four of forty-eight available satellites. Both Russian GLONASS and American NAVSTAR satellite constellations are used to calculate the position and to provide real time guidance to the helicopter. For flight path processing an Ashtech Z-surveyor was used as the mobile receiver. A Novatel Millennium duel frequency system was used as the primary base station receiver. The base

station was located at WGS84 LAT 29° 42' 54.72030" N and LON 98° 36' 52.90654" W at 368.8 metres above the ellipsoid. The mobile and base station raw XYZ data were recorded, thereby permitting post-survey differential corrections for theoretical accuracies of better than 2 metres. A Marconi Allstar GPS unit was used as a secondary (back-up) base station.

Radar Altimeter

Manufacturer:	Honeywell/Sperry
Model:	RT330
Type:	Short pulse modulation, 4.3 GHz
Sensitivity:	0.3 m

The radar altimeter measures the vertical distance between the helicopter and the ground. This information is used in the processing algorithm that determines conductor depth.

Barometric Pressure and Temperature Sensors

Model:	DIGHEM D 1300	
Type:	Motorola MPX4115AP analog pressure sensor	
	AD592AN high-impedance remote temperature sensors	
Sensitivity:	Pressure:	150 mV/kPa
	Temperature:	100 mV/°C or 10 mV/°C (selectable)
Sample rate:	10 per second	

The D1300 circuit is used in conjunction with one barometric sensor and up to three temperature sensors. Two sensors (baro and temp) are installed in the EM console in the aircraft, to monitor pressure and internal operating temperatures.

Laser Altimeter

Manufacturer:	Optech

Model:	G150
Type:	Fixed pulse repetition rate of 2 kHz
Sensitivity:	±5 cm from 10ºC to 30ºC
	±10 cm from -20ºC to +50ºC

The laser altimeter is housed in the EM bird, and measures the distance from the EM bird to ground, except in areas of dense tree cover.

Analog Recorder

Manufacturer:	RMS Instruments
Type:	DGR33 dot-matrix graphics recorder
Resolution:	4x4 dots/mm
Speed: 1.5 mm/sec	

The analog profiles are recorded on chart paper in the aircraft during the survey. Table 3-1 lists the geophysical data channels and the vertical scale of each profile.

Digital Data Acquisition System

Manufacturer:	RMS Instruments
Model:	DGR 33
Recorder:	San Disk compact flash card (PCMCIA)

The data are stored on flash cards and are downloaded to the field workstation PC at the survey base for verification, backup and preparation of in-field products.

Flight Path Video Recording System

Recorder: Panasonic AG-720

Fiducial numbers are recorded continuously and are displayed on the margin of each image. This procedure ensures accurate correlation of analog and digital data with respect to visible features on the ground.

Table 3-1. The Analog Profiles

Channel Name	Parameter	Scale units/mm
400I	coaxial in-phase (400 Hz)	5 ppm
400Q	coaxial quad (400 Hz)	5 ppm
1K5I	coplanar in-phase (1500 Hz)	5 ppm
1K5Q	coplanar quad (1500 Hz)	5 ppm
1X8I	coaxial in-phase (3300 Hz)	5 ppm
1X8Q	coaxial quad (3300 Hz)	5 ppm
6K2I	coplanar in-phase (6200 Hz)	10 ppm
6K2Q	coplanar quad (6200 Hz)	10 ppm
25KI	coplanar in-phase (25,000 Hz)	40 ppm
25KQ	coplanar quad (25,000 Hz)	40 ppm
100I	coplanar inphase (115,000 Hz)	40 ppm
100Q	coplanar quad (115,000 Hz)	40 ppm
ALTL	altimeter (laser)	3 m
ALTR	altimeter (radar)	3 m
MAG1	magnetics, coarse	20 nT
1SP	coaxial spherics monitor	
2SP	coplanar spherics monitor	
2PL	coplanar powerline monitor	
1KPA	altimeter (barometric)	30 m
2TDC	internal (console) temperature	1° C
3TDC	external temperature	1° C

4. QUALITY CONTROL AND IN-FIELD PROCESSING

Digital data for each flight were transferred to the field workstation, in order to verify data quality and completeness. A database was created and updated using Geosoft Oasis Montaj and proprietary Fugro Atlas software. This allowed the field personnel to calculate, display and verify both the positional (flight path) and geophysical data on a screen or printer. Analog records were examined as a preliminary assessment of the data acquired for each flight.

In-field processing of Fugro survey data consists of differential corrections to the airborne GPS data, verification of EM calibrations, drift correction of the raw airborne EM data, spike rejection and filtering of all geophysical and ancillary data, verification of flight videos, calculation of preliminary resistivity data, diurnal correction, and preliminary leveling of magnetic data.

All data, including base station records, were checked on a daily basis, to ensure compliance with the survey contract specifications. Reflights were required if any of the standard specifications were not met.

5. DATA PROCESSING

Flight Path Recovery

The raw range data from at least four satellites are simultaneously recorded by both the base and mobile GPS units. The geographic positions of both units, relative to the model ellipsoid, are calculated from this information. Differential corrections, which are obtained from the base station, are applied to the mobile unit data to provide a post-flight track of the aircraft, accurate to within 2 m. Speed checks of the flight path are also carried out to determine if there are any spikes or gaps in the data.

The corrected WGS84 latitude/longitude coordinates are transformed to the coordinate system used on the final maps. Images or plots are then created to provide a visual check of the flight path.

Electromagnetic Data/Apparent Resistivity

EM data are processed at the recorded sample rate of 10 samples/second. Spheric rejection median and Hanning filters were applied to reduce noise to acceptable levels.

The apparent resistivity in ohm-m were generated from the in-phase and quadrature EM components for all of the coplanar frequencies, using a pseudo-layer half-space model. The inputs to the resistivity algorithm are the inphase and quadrature amplitudes of the secondary field. The algorithm calculates the apparent resistivity in ohm-m, and the apparent height of the bird above the conductive source. Any difference between the apparent height and the true height, as measured by the radar altimeter, is called the pseudo-layer and reflects the difference between the real geology and a homogeneous halfspace. This difference is often attributed to the presence of a highly resistive upper layer. Any errors in the altimeter reading, caused by heavy tree cover, are included in the pseudo-layer and do not affect the resistivity calculation. The apparent depth estimates, however, will reflect the altimeter errors. Apparent resistivity calculated in this manner may behave quite differently from those calculated using other models.

In areas of high magnetic permeability or dielectric permittivity, the calculated resistivities will be erroneously high. Various algorithms and inversion techniques can be used to partially correct for this effect.

The preliminary apparent resistivity maps and images were carefully inspected to identify any lines or line segments that might require base level adjustments. Subtle changes between in-flight calibrations of the system can result in line-to-line differences that are more recognizable in resistive (low signal amplitude) areas. Manual leveling was carried out to eliminate or minimize resistivity differences that can be attributed, in part, to changes in operating temperatures. These leveling adjustments were usually very subtle, and do not result in the degradation of discrete anomalies.

After the manual leveling process is complete, the data were subjected to a microleveling technique in order to remove any remaining line-to-line differences within the calculated resistivities.

Apparent resistivity grids, which display the conductive properties of the survey areas, were produced from the 400 Hz, 1500 Hz, 6400 Hz, 25,000 Hz and 115,000 Hz coplanar data. The calculated resistivities for the five coplanar frequencies are included in the XYZ and grid archives. Values are in ohm-metres on all final products.

Total Magnetic Field

The aeromagnetic data were inspected in grid and profile format. Spikes were removed manually with the aid of a fourth difference calculation. A Geometrics G822 cesium vapour magnetometer was operated at the survey base to record diurnal variations of the earth's magnetic field. The clock of the base station was synchronized with that of the airborne system to permit subsequent removal of diurnal drift. The data were inspected for spikes and filtered. The filtered diurnal data were subtracted from the total field magnetic data. Grids of the diurnally corrected aeromagnetic data were created and contoured. A lag correction was applied to the magnetic data. The results were then leveled using tie and traverse line intercepts. Manual adjustments were applied to any lines that required leveling, as indicated by shadowed images of both the total

field magnetic data and the calculated vertical gradient data. A microleveling algorithm was used to make any remaining subtle leveling adjustments.

Contour, Colour and Shadow Map Displays

The geophysical data are interpolated onto a regular grid using a modified Akima spline technique. The resulting grid is suitable for image processing and generation of contour maps. The grid cell size was 20% of the line interval; 40 metres for the 200 metre spaced portion of the survey area, 20 metres for the 100 metre spaced detail area.

Colour maps are produced by interpolating the grid down to the pixel size. The parameter is then incremented with respect to specific amplitude ranges to provide colour "contour" maps.

Monochromatic shadow maps or images can be generated by employing an artificial sun to cast shadows on a surface defined by the geophysical grid. There are many variations in the shadowing technique. These techniques can be applied to total field or enhanced magnetic data, magnetic derivatives, resistivity, etc. The shadowing technique is also used as a quality control method to detect subtle changes between lines.

Resistivity-depth Sections

The apparent resistivities for all frequencies can be displayed simultaneously as coloured resistivity-depth sections. Usually, only the coplanar data are displayed as the close frequency separation between the coplanar and adjacent coaxial data tends to distort the section. The sections can be plotted using the topographic elevation profile as the surface. The digital terrain values, in metres a.m.s.l., can be calculated from the GPS Z-value or barometric altimeter, minus the aircraft radar altimeter.

Resistivity-depth sections can be generated in three formats:

(1) Sengpiel resistivity sections, where the apparent resistivity for each frequency is plotted at the depth of the centroid of the in-phase current flow[1]; and,

(2) Differential resistivity sections, where the differential resistivity is plotted at the differential depth[2].

(3) Occam[3] or Multi-layer[4] inversion.

Both the Sengpiel and differential methods are derived from the pseudo-layer half-space model. Both yield a coloured resistivity-depth section that attempts to portray a smoothed approximation of the true resistivity distribution with depth. Resistivity-depth sections are most useful in conductive layered situations, but may be unreliable in areas of moderate to high resistivity where signal amplitudes are weak. In areas where in-phase responses have been suppressed by the effects of magnetite, or adversely affected by cultural features, the computed resistivities shown on the sections may be unreliable.

Both the Occam and multi-layer inversions compute the layered earth resistivity model that would best match the measured EM data. The Occam inversion uses a series of thin, fixed layers (usually 20 x 5m and 10 x 10m layers) and computes resistivities to fit the EM data. The multi-layer

---

[1] Sengpiel, K.P., 1988, Approximate Inversion of Airborne EM Data from Multilayered Ground: Geophysical Prospecting 36, 446-459.

[2] Huang, H. and Fraser, D.C., 1993, Differential Resistivity Method for Multi-frequency Airborne EM Sounding: presented at Intern. Airb. EM Workshop, Tucson, Ariz.

[3] Constable et al, 1987, Occam's inversion: a practical algorithm for generating smooth models from electromagnetic sounding data: Geophysics, 52, 289-300.

[4] Huang H., and Palacky, G.J., 1991, Damped least-squares inversion of time domain airborne EM data based on singular value decomposition: Geophysical Prospecting, 39, 827-844.

inversion computes the resistivity and thickness for each of a defined number of layers (typically 3-5 layers) to best fit the data.

6. PRODUCTS

This section lists the final maps and products that have been provided under the terms of the survey agreement. Other products can be prepared from the existing dataset, if requested. These include magnetic enhancements or derivatives, percent magnetite, resistivities corrected for magnetic permeability and/or dielectric permittivity, digital terrain, resistivity-depth sections, inversions, and overburden thicknesses.

Base Maps

Base maps of the survey area were produced by scanning published topographic maps to a TIF format. This process provides a relatively accurate, distortion free base that facilitates correlation of the navigation data to the map coordinate system. The topographic files were combined with geophysical data for plotting the final maps. All maps were created using the following parameters:

Projection Description:

Datum:	NAD 27
Ellipsoid:	Clarke 1866
DX,DY,ZY shift	8 -159 -175
Projection:	UTM (Zone: 14)
Central Meridian:	99° West
False Northing:	0
False Easting:	500000
Scale Factor:	0.9996

The following parameters are presented on 1 map sheet for each target, at a scale of 1:24,000. Preliminary products are not listed.

Final Products

Colour Maps (2 copies) at 1:24000

Apparent Resistivity 400 Hz
Apparent Resistivity 1500 Hz
Apparent Resistivity 6200 Hz
Apparent Resistivity 25,000 Hz
Apparent Resistivity 115,000 Hz

Black & White Maps at 1:24000 (Mylar)

Total Magnetic Field maps

Additional Products

Digital Archive on CD-ROM	2 copies
Survey Report	2 copies
Analog Chart Records	All flights
Flight Path Video (VHS)	All flights
Flight Path Video (DVD)	All flights

7. CONCLUSIONS AND RECOMMENDATIONS

This report provides a description of the equipment, data processing procedures and logistics of the survey.

The various maps included with this report display the magnetic and conductive properties of the survey area. It is recommended that a complete assessment and detailed evaluation of the survey results be carried out, in conjunction with all available geophysical, geological and geochemical information.

It is also recommended that image processing of existing geophysical data be considered, in order to extract the maximum amount of information from the survey results. Current software and imaging techniques often provide valuable information on structure and lithology, which may not be clearly evident on the contour and colour maps. These techniques can yield images that define subtle, but significant, structural details.

Respectfully submitted,

FUGRO AIRBORNE SURVEYS CORP.

Michael Cain, P. Eng.
Geophysicist

APPENDIX A
LIST OF PERSONNEL

The following personnel were involved in the acquisition, processing, interpretation and presentation of data, relating to a RESOLVE airborne geophysical survey carried out for the U. S. Geological Survey, over northern Bexar County, Texas

David Miles	Manager, Helicopter Operations
Emily Farquhar	Manager, Data Processing and Interpretation
Bill Brown	Sales and Marketing
Michael Cain	Project Geophysicist
Elizabeth Bowslaugh	Data processor
Darcy Blouin	Geophysical Operator
Terry Thomson	Pilot (Questral Helicopters Ltd.)
Lyn Vanderstarren	Drafting Supervisor
Albina Tonello	Secretary/Expeditor

The survey consisted of 1281 km of coverage, flown from December 10th to 14th, 2003.

All personnel are employees of Fugro Airborne Surveys, except for the pilot who is an employee of Questral Helicopters Ltd.

APPENDIX B
ARCHIVE DESCRIPTION

This CD-ROM contains final data archives of an airborne survey conducted by Fugro Airborne Surveys on behalf of the U. S. Geological Survey. The survey was flown from December 10th to 14th, 2003.

Fugro Job #03069

CD Archive number: CCD02102

Fugro Airborne Surveys Job #03069

The archives contain three directories.

1. Line Data: Geosoft GDB database with archive description.

2. Grids: Grids in Geosoft GRD format for the following parameters:
    1. Magnetic total field (IGRF corrected)
    2. 5 coplanar resistivities

3. Report: A digital copy of the operations report in PDF format

Projection Description:

Datum:	NAD27
Ellipsoid:	Clarke 1866
Projection:	UTM (Zone: 14)
Central Meridian:	99º West

- Appendix B.2 -

False Northing:	0
False Easting:	500000
Scale Factor:	0.9996
WGS84 to Local Conversion:	Molodensky
X,Y,Z Datum Shifts:	8 -159 -175

- Appendix B.3 -

EM PARAMETERS

orientation	nominal	FREQUENCY actual	COIL SPACING
coplanar	400 Hz	389 Hz	7.9 m
coplanar	1 500 Hz	1 574 Hz	7.9 m
coaxial	3 300 Hz	3 245 Hz	9.0 m
coplanar	6 200 Hz	6 075 Hz	7.9 m
coplanar	25 000 Hz	25 300 Hz	7.9 m
coplanar	115 000 Hz	114 940 Hz	7.9 m

DATABASE : 03069_BEXAR.GDB

==========

NUMBER OF DATABASE CHANNELS : 99

==========

1	ALTBIRDM	BIRD RADAR ALTIMETER (METRES)
2	ALTBIRDR	BIRD RADAR ALTIMETER RAW (METRES)
3	ALTLASM	BIRD LASER ALTIMETER PROCESSED (METRES)
4	ALTLASR	BIRD LASER ALTIMETER RAW (METRES)
5	BALT	BAROMETRIC ALTIMETER RAW (METRES)
6	CEN115k	CENTROID DEPTH 115K HZ
7	CEN1500	CENTROID DEPTH 1500 HZ
8	CEN25k	CENTROID DEPTH 25K HZ
9	CEN400	CENTROID DEPTH 400 HZ
10	CEN6200	CENTROID DEPTH 6200 HZ
11	CPI115K	COPLANAR INPHASE FULLY PROCESSED 115K HZ
12	CPI1500	COPLANAR INPHASE FULLY PROCESSED 1500 HZ
13	CPI25K	COPLANAR INPHASE FULLY PROCESSED 25K HZ
14	CPI400	COPLANAR INPHASE FULLY PROCESSED 400 HZ
15	CPI6200	COPLANAR INPHASE FULLY PROCESSED 6200 HZ
16	CPQ115K	COPLANAR QUADRATURE FULLY PROCESSED 115K HZ
17	CPQ1500	COPLANAR QUADRATURE FULLY PROCESSED 1500 HZ
18	CPQ25K	COPLANAR QUADRATURE FULLY PROCESSED 25K HZ
19	CPQ400	COPLANAR QUADRATURE FULLY PROCESSED 400 HZ
20	CPQ6200	COPLANAR QUADRATURE FULLY PROCESSED 6200 Hz
21	CXI3300	COAXIAL INPHASE FULLY PROCESSED 3300 HZ
22	CXQ3300	COAXIAL QUADRATURE FULLY PROCESSED 3300 HZ
23	CPPL	COPLANAR POWERLINE MONITOR
24	CXPL	COAXIAL POWERLINE MONITOR

- Appendix B.4 -

25	Date	FLIGHT DATE
26	DDEP115K	DIFFERENTIAL DEPTH 115K HZ FILTERED
27	DDEP1500	DIFFERENTIAL DEPTH 1500HZ FILTERED
28	DDEP25K	DIFFERENTIAL DEPTH 25K HZ FILTERED
29	DDEP400	DIFFERENTIAL DEPTH 400 HZ FILTERED
30	DDEP6200	DIFFERENTIAL DEPTH 6200 HZ FILTERED
31	DEP115K	APPARENT DEPTH 115K HZ FILTERED
32	DEP1500	APPARENT DEPTH 1500HZ FILTERED
33	DEP25K	APPARENT DEPTH 25K HZ FILTERED
34	DEP3300	APPARENT DEPTH 3300 HZ FILTERED
35	DEP400	APPARENT DEPTH 400 HZ FILTERED
36	DEP6200	APPARENT DEPTH 6200 HZ FILTERED
37	DIURNAL	DIURNAL CORRECTION
38	DRES115K	DIFFERENTIAL RESISTIVITY 115K HZ FILTERED
39	DRES1500	DIFFERENTIAL RESISTIVITY 1500 HZ FILTERED
40	DRES25K	DIFFERENTIAL RESISTIVITY 25K HZ FILTERED
41	DRES400	DIFFERENTIAL RESISTIVITY 400 HZ FILTERED
42	DRES6200	DIFFERENTIAL RESISTIVITY 6200 HZ FILTERED
43	DTM	DIGITAL TERRAIN MODEL
44	FID	FIDUCIAL COUNTER
45	Flight	FLIGHT NUMBER
46	GPSZ4	RAW GPS ELEVATION
47	L100I	BASE LEVELED INPHASE 115K HZ
48	L100Q	BASE LEVELED QUADRATURE 115K HZ
49	L1K5I	BASE LEVELED INPHASE 1500 HZ
50	L1K5Q	BASE LEVELED QUADRATURE 1500 HZ
51	L1K7I	BASE LEVELED INPHASE 3300 HZ
52	L1K7Q	BASE LEVELED QUADRATURE 3300 HZ
53	L25KI	BASE LEVELED INPHASE 25K HZ
54	L25KQ	BASE LEVELED QUADRATURE 25K HZ
55	L400I	BASE LEVELED INPHASE 400 HZ
56	L400Q	BASE LEVELED QUADRATURE 400 HZ
57	L6K2I	BASE LEVELED INPHASE 6200 HZ
58	L6K2Q	BASE LEVELED QUADRATURE 6200 HZ
59	LAT	WGS84 LATITUDE
60	LON	WGS84 LONGITUDE
61	LINE	LINE NUMBER
62	MAGD	DIURNAL CORRECTED MAG
63	MAGRAW	RAW MAG
64	MAG_GL	MAG MICROLEVELED
65	MAG_IGRFZ	MAG IGRF REMOVED USING Z ALTITUDE
66	MAG_LEVEL	TIE LINE LEVELED MAG
67	TMI	MAG Final

```
   68 - RES115K           RESISTIVITY 115K HZ
   69 - RES1500           RESISTIVITY 1500 HZ
   70 - RES25K            RESISTIVITY 25K HZ
   71 - RES3300           RESISTIVITY 3300 HZ
   72 - RES400            RESISTIVITY 400 HZ F
   73 - RES6200_filt      RESISTIVITY 6200 HZ
   74 - RES115K_filt      RESISTIVITY 115K HZ FILTERED
   75 - RES1500_filt      RESISTIVITY 1500 HZ FILTERED
   76 - RES25K_filt       RESISTIVITY 25K HZ FILTERED
   77 - RES400_filt       RESISTIVITY 400 HZ FILTERED
   78 - RES6200_filt      RESISTIVITY 6200 HZ FILTERED
   79 - UTC               UTC TIME
   80 - X                 FINAL BIRD UTM X CLARK 1866 (NAD27)
   81 - X4                RAW BIRD UTM X CLARK 1866 (NAD27)
   82 - Y                 FINAL UTM Y CLARK 1866 (NAD27)
   83 - Y4                RAW UTM Y CLARK 1866 (NAD27)
   84 - X_HELI            UTM X FROM HELI GPS CLARK 1866 (NAD27)
   85 - Y_HELI            UTM X FROM HELI GPS CLARK 1866 (NAD27)
   86 - Z                 FINAL GPS ELEVATION
   87 - _100I             RAW INPHASE 115K HZ
   88 - _100Q             RAW QUADRATURE 115K HZ
   89 - _1K5I             RAW INPHASE 1500 HZ
   90 - _1K5Q             RAW QUADRATURE 1500 HZ
   91 - _1K7I             RAW INPHASE 3300 HZ
   92 - _1K7Q             RAW QUADRATURE 3300 HZ
   93 - _25KI             RAW INPHASE 25K HZ
   94 - _25KQ             RAW QUADRATURE 25K HZ
   95 - _400I             RAW INPHASE 400 HZ
   96 - _400Q             RAW QUADRATURE 400 HZ
   97 - _6K2I             RAW INPHASE 6200 HZ
   98 - _6K2Q             RAW QUADRATURE 6200 HZ
=====================================================
```

APPENDIX C

BACKGROUND INFORMATION

Electromagnetics

Fugro electromagnetic responses fall into two general classes, discrete and broad. The discrete class consists of sharp, well-defined anomalies from discrete conductors such as sulphide lenses and steeply dipping sheets of graphite and sulphides. The broad class consists of wide anomalies from conductors having a large horizontal surface such as flatly dipping graphite or sulphide sheets, saline water-saturated sedimentary formations, conductive overburden and rock, kimberlite pipes and geothermal zones. A vertical conductive slab with a width of 200 m would straddle these two classes.

The vertical sheet (half plane) is the most common model used for the analysis of discrete conductors. All anomalies plotted on the geophysical maps are analyzed according to this model. The following section entitled **Discrete Conductor Analysis** describes this model in detail, including the effect of using it on anomalies caused by broad conductors such as conductive overburden.

The conductive earth (half-space) model is suitable for broad conductors. Resistivity contour maps result from the use of this model. A later section entitled **Resistivity Mapping** describes the method further, including the effect of using it on anomalies caused by discrete conductors such as sulphide bodies.

Geometric Interpretation

The geophysical interpreter attempts to determine the geometric shape and dip of the conductor. Figure C-1 shows typical HEM anomaly shapes which are used to guide the geometric interpretation.

Discrete Conductor Analysis

- Appendix C.2 -

The EM anomalies appearing on the electromagnetic map are analyzed by computer to give the conductance (i.e., conductivity-thickness product) in siemens (mhos) of a vertical sheet model. This is done regardless of the interpreted geometric shape of the conductor. This is not an unreasonable procedure, because the computed conductance increases as the electrical quality of the conductor increases, regardless of its true shape. DIGHEM anomalies are divided into seven grades of conductance, as shown in Table C-1. The conductance in siemens (mhos) is the reciprocal of resistance in ohms.

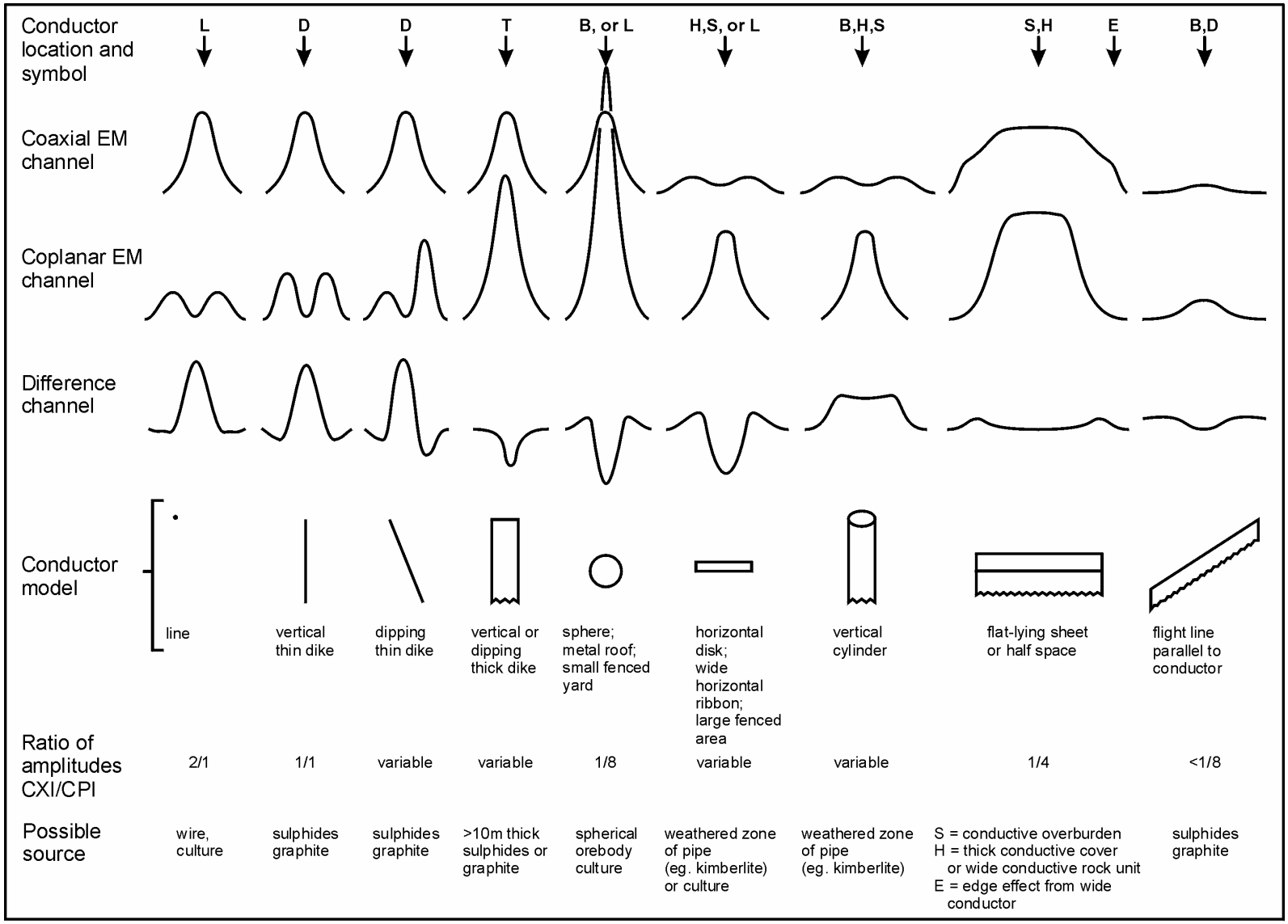

Typical DIGHEM anomaly shapes

Figure C-1

The conductance value is a geological parameter because it is a characteristic of the conductor alone. It generally is independent of frequency, flying height or depth of burial, apart from the averaging over a greater portion of the conductor as height increases. Small anomalies from deeply buried strong conductors are not confused with small anomalies from shallow weak conductors because the former will have larger conductance values.

Table C-1. EM Anomaly Grades

Anomaly Grade	Siemens
7	> 100
6	50 - 100
5	20 - 50
4	10 - 20
3	5 - 10
2	1 - 5
1	< 1

Conductive overburden generally produces broad EM responses which may not be shown as anomalies on the geophysical maps. However, patchy conductive overburden in otherwise resistive areas can yield discrete anomalies with a conductance grade (cf. Table C-1) of 1, 2 or even 3 for conducting clays which have resistivities as low as 50 ohm-m. In areas where ground resistivities are below 10 ohm-m, anomalies caused by weathering variations and similar causes can have any conductance grade. The anomaly shapes from the multiple coils often allow such conductors to be recognized, and these are indicated by the letters S, H, and sometimes E on the geophysical maps (see EM legend on maps).

For bedrock conductors, the higher anomaly grades indicate increasingly higher conductances. Examples: the New Insco copper discovery (Noranda, Canada) yielded a grade 5 anomaly, as did the neighbouring copper-zinc Magusi River ore body; Mattabi (copper-zinc, Sturgeon Lake, Canada) and Whistle (nickel, Sudbury, Canada) gave grade 6; and the Montcalm nickel-copper discovery (Timmins, Canada) yielded a grade 7 anomaly. Graphite and sulphides can span all grades but, in any particular survey area, field work may show that the different grades indicate different types of conductors.

Strong conductors (i.e., grades 6 and 7) are characteristic of massive sulphides or graphite. Moderate conductors (grades 4 and 5) typically reflect graphite or sulphides of a less massive character, while weak bedrock conductors (grades 1 to 3) can signify poorly connected graphite or heavily disseminated sulphides. Grades 1 and 2 conductors may not respond to ground EM equipment using frequencies less than 2000 Hz.

The presence of sphalerite or gangue can result in ore deposits having weak to moderate conductances. As an example, the three million ton lead-zinc deposit of Restigouche Mining Corporation near Bathurst, Canada, yielded a well-defined grade 2 conductor. The 10 percent by volume of sphalerite occurs as a coating around the fine grained massive pyrite, thereby inhibiting electrical conduction. Faults, fractures and shear zones may produce anomalies that typically have low conductances (e.g., grades 1 to 3). Conductive rock formations can yield anomalies of any conductance grade. The conductive materials in such rock formations can be salt water, weathered products such as clays, original depositional clays, and carbonaceous material.

For each interpreted electromagnetic anomaly on the geophysical maps, a letter identifier and an interpretive symbol are plotted beside the EM grade symbol. The horizontal rows of dots, under the interpretive symbol, indicate the anomaly amplitude on the flight record. The vertical column of dots, under the anomaly letter, gives the estimated depth. In areas where anomalies are crowded, the letter identifiers, interpretive symbols and dots may be obliterated. The EM grade symbols, however, will always be discernible, and the obliterated information can be obtained from the anomaly listing appended to this report.

The purpose of indicating the anomaly amplitude by dots is to provide an estimate of the reliability of the conductance calculation. Thus, a conductance value obtained from a large ppm anomaly (3 or 4 dots) will tend to be accurate whereas one obtained from a small ppm anomaly (no dots) could be quite inaccurate. The absence of amplitude dots indicates that the anomaly from the coaxial coil-pair is 5 ppm or less on both the in-phase and quadrature channels. Such small anomalies could reflect a weak conductor at the surface or a stronger conductor at depth. The conductance grade and depth estimate illustrates which of these possibilities fits the recorded data best.

The conductance measurement is considered more reliable than the depth estimate. There are a number of factors that can produce an error in the depth estimate, including the averaging of topographic variations by the altimeter, overlying conductive overburden, and the location and attitude of the conductor relative to the flight line. Conductor location and attitude can provide an erroneous depth estimate because the stronger part of the conductor may be deeper or to one side of the flight line, or because it has a shallow dip. A heavy tree cover can also produce errors in depth estimates. This is because the depth estimate is computed as the distance of bird from conductor, minus the altimeter reading. The altimeter can lock onto the top of a dense forest canopy. This situation yields an erroneously large depth estimate but does not affect the conductance estimate.

Dip symbols are used to indicate the direction of dip of conductors. These symbols are used only when the anomaly shapes are unambiguous, which usually requires a fairly resistive environment.

A further interpretation is presented on the EM map by means of the line-to-line correlation of bedrock anomalies, which is based on a comparison of anomaly shapes on adjacent lines. This provides conductor axes that may define the geological structure over portions of the survey area. The absence of conductor axes in an area implies that anomalies could not be correlated from line to line with reasonable confidence.

The electromagnetic anomalies are designed to provide a correct impression of conductor quality by means of the conductance grade symbols. The symbols can stand alone with geology when planning a follow-up program. The actual conductance values are printed in the attached anomaly list for those who wish quantitative data. The anomaly ppm and depth are indicated by inconspicuous dots which should not distract from the conductor patterns, while being helpful to those who wish this information. The map provides an interpretation of conductors in terms of length, strike and dip, geometric shape, conductance, depth, and thickness. The accuracy is comparable to an interpretation from a high quality ground EM survey having the same line spacing.

The appended EM anomaly list provides a tabulation of anomalies in ppm, conductance, and depth for the vertical sheet model. No conductance or depth estimates are shown for weak anomalous responses that are not of sufficient amplitude to yield reliable calculations.

Since discrete bodies normally are the targets of EM surveys, local base (or zero) levels are used to compute local anomaly amplitudes. This contrasts with the use of true zero levels which are used to compute true EM amplitudes. Local anomaly amplitudes are shown in the EM anomaly list and these are used to compute the vertical sheet parameters of conductance and depth.

Questionable Anomalies

The EM maps may contain anomalous responses that are displayed as asterisks (*). These responses denote weak anomalies of indeterminate conductance, which may reflect one of the following: a weak conductor near the surface, a strong conductor at depth (e.g., 100 to 120 m below surface) or to one side of the flight line, or aerodynamic noise. Those responses that have the appearance of valid bedrock anomalies on the flight profiles are indicated by appropriate interpretive symbols (see EM legend on maps). The others probably do not warrant further investigation unless their locations are of considerable geological interest.

The Thickness Parameter

A comparison of coaxial and coplanar shapes can provide an indication of the thickness of a steeply dipping conductor. The amplitude of the coplanar anomaly (e.g., CPI channel) increases relative to the coaxial anomaly (e.g., CXI) as the apparent thickness increases, i.e., the thickness in the horizontal plane. (The thickness is equal to the conductor width if the conductor dips at 90 degrees and strikes at right angles to the flight line.) This report refers to a conductor as thin when the thickness is likely to be less than 3 m, and thick when in excess of 10 m. Thick conductors are indicated on the EM map by parentheses "( )". For base metal exploration in steeply dipping geology, thick conductors can be high priority targets because many massive sulphide ore bodies are thick. The system cannot sense the thickness when the strike of the conductor is subparallel to the flight line, when the conductor has a shallow dip, when the anomaly amplitudes are small, or when the resistivity of the environment is below 100 ohm-m.

Resistivity Mapping

Resistivity mapping is useful in areas where broad or flat lying conductive units are of interest. One example of this is the clay alteration which is associated with Carlin-type deposits in the south west United States. The resistivity parameter was able to identify the clay alteration zone over the Cove deposit. The alteration zone appeared as a strong resistivity low on the 900 Hz resistivity parameter. The 7,200 Hz and 56,000 Hz resistivities showed more detail in the covering sediments, and delineated a range front fault. This is typical in many areas of the south west United States, where conductive near surface sediments, which may sometimes be alkalic, attenuate the higher frequencies.

Resistivity mapping has proven successful for locating diatremes in diamond exploration. Weathering products from relatively soft kimberlite pipes produce a resistivity contrast with the unaltered host rock. In many cases weathered kimberlite pipes were associated with thick conductive layers that contrasted with overlying or adjacent relatively thin layers of lake bottom sediments or overburden.

Areas of widespread conductivity are commonly encountered during surveys. These conductive zones may reflect alteration zones, shallow-dipping sulphide or graphite-rich units, saline ground water, or conductive overburden. In such areas, EM amplitude changes can be generated by decreases of only 5 m in survey altitude, as well as by increases in conductivity. The typical flight record in conductive areas is characterized by in-phase and quadrature channels that are continuously active. Local EM peaks reflect either increases in conductivity of the earth or decreases in survey altitude. For such conductive areas, apparent resistivity profiles and contour maps are necessary for the correct interpretation of the airborne data. The advantage of the resistivity parameter is that anomalies caused by altitude changes are virtually eliminated, so the resistivity data reflect only those anomalies caused by conductivity changes. The resistivity analysis also helps the interpreter to differentiate between conductive bedrock and conductive overburden. For example, discrete conductors will generally appear as narrow lows on the contour map and broad conductors (e.g., overburden) will appear as wide lows.

The apparent resistivity is calculated using the pseudo-layer (or buried) half-space model defined by Fraser (1978)[5]. This model consists of a resistive layer overlying a conductive half-space. The depth channels give the apparent depth below surface of the conductive material. The apparent depth is simply the apparent thickness of the overlying resistive layer. The apparent depth (or thickness) parameter will be positive when the upper layer is more resistive than the underlying material, in which case the apparent depth may be quite close to the true depth.

The apparent depth will be negative when the upper layer is more conductive than the underlying material, and will be zero when a homogeneous half-space exists. The apparent depth parameter must be interpreted cautiously because it will contain any errors that might exist in the measured altitude of the EM bird (e.g., as caused by a dense tree cover). The inputs to the resistivity algorithm are the in-phase and quadrature components of the coplanar coil-pair. The outputs are the apparent resistivity of the conductive half-space (the source) and the sensor-source distance. The flying height is not an input variable, and the output resistivity and sensor-source distance are independent of the flying height when the conductivity of the measured material is sufficient to yield significant in-phase as well as quadrature responses. The apparent depth, discussed above, is simply the sensor-source distance minus the measured altitude or flying height. Consequently, errors in the measured altitude will affect the apparent depth parameter but not the apparent resistivity parameter.

The apparent depth parameter is a useful indicator of simple layering in areas lacking a heavy tree cover. Depth information has been used for permafrost mapping, where positive apparent depths were used as a measure of permafrost thickness. However, little quantitative use has been made of negative apparent depths because the absolute value of the negative depth is not a measure of the thickness of the conductive upper layer and, therefore, is not meaningful physically. Qualitatively, a negative apparent depth estimate usually shows that the EM anomaly is caused by conductive overburden. Consequently, the apparent depth channel can be of significant help in distinguishing between overburden and bedrock conductors.

---

[5] Resistivity mapping with an airborne multicoil electromagnetic system: Geophysics, v. 43, p.144-172

Interpretation in Conductive Environments

Environments having low background resistivities (e.g., below 30 ohm-m for a 900 Hz system) yield very large responses from the conductive ground. This usually prohibits the recognition of discrete bedrock conductors. However, Fugro data processing techniques produce three parameters that contribute significantly to the recognition of bedrock conductors in conductive environments. These are the in-phase and quadrature difference channels (DIFI and DIFQ, which are available only on systems with "common" frequencies on orthogonal coil pairs), and the resistivity and depth channels (RES and DEP) for each coplanar frequency.

The EM difference channels (DIFI and DIFQ) eliminate most of the responses from conductive ground, leaving responses from bedrock conductors, cultural features (e.g., telephone lines, fences, etc.) and edge effects. Edge effects often occur near the perimeter of broad conductive zones. This can be a source of geologic noise. While edge effects yield anomalies on the EM difference channels, they do not produce resistivity anomalies. Consequently, the resistivity channel aids in eliminating anomalies due to edge effects. On the other hand, resistivity anomalies will coincide with the most highly conductive sections of conductive ground, and this is another source of geologic noise. The recognition of a bedrock conductor in a conductive environment therefore is based on the anomalous responses of the two difference channels (DIFI and DIFQ) and the resistivity channels (RES). The most favourable situation is where anomalies coincide on all channels.

The DEP channels, which give the apparent depth to the conductive material, also help to determine whether a conductive response arises from surficial material or from a conductive zone in the bedrock. When these channels ride above the zero level on the depth profiles (i.e., depth is negative), it implies that the EM and resistivity profiles are responding primarily to a conductive upper layer, i.e., conductive overburden. If the DEP channels are below the zero level, it indicates that a resistive upper layer exists, and this usually implies the existence of a bedrock conductor. If the low frequency DEP channel is below the zero level and the high frequency DEP is above, this suggests that a bedrock conductor occurs beneath conductive cover.

Reduction of Geologic Noise

Geologic noise refers to unwanted geophysical responses. For purposes of airborne EM surveying, geologic noise refers to EM responses caused by conductive overburden and magnetic permeability. It was mentioned previously that the EM difference channels (i.e., channel DIFI for in-phase and DIFQ for quadrature) tend to eliminate the response of conductive overburden.

Magnetite produces a form of geological noise on the in-phase channels. Rocks containing less than 1% magnetite can yield negative in-phase anomalies caused by magnetic permeability. When magnetite is widely distributed throughout a survey area, the in-phase EM channels may continuously rise and fall, reflecting variations in the magnetite percentage, flying height, and overburden thickness. This can lead to difficulties in recognizing deeply buried bedrock conductors, particularly if conductive overburden also exists. However, the response of broadly distributed magnetite generally vanishes on the in-phase difference channel DIFI. This feature can be a significant aid in the recognition of conductors that occur in rocks containing accessory magnetite.

EM Magnetite Mapping

The information content of HEM data consists of a combination of conductive eddy current responses and magnetic permeability responses. The secondary field resulting from conductive eddy current flow is frequency-dependent and consists of both in-phase and quadrature components, which are positive in sign. On the other hand, the secondary field resulting from magnetic permeability is independent of frequency and consists of only an in-phase component that is negative in sign. When magnetic permeability manifests itself by decreasing the measured amount of positive in-phase, its presence may be difficult to recognize. However, when it manifests itself by yielding a negative in-phase anomaly (e.g., in the absence of eddy current flow), its presence is assured. In this latter case, the negative component can be used to estimate the percent magnetite content.

A magnetite mapping technique, based on the low frequency coplanar data, can be complementary to magnetometer mapping in certain cases. Compared to magnetometry, it is far less sensitive but is more able to resolve closely spaced magnetite zones, as well as providing an estimate of the amount of magnetite in the rock. The method is sensitive to 1/4% magnetite by weight when the EM sensor is at a height of 30 m above a magnetitic half-space. It can individually resolve steep dipping narrow

magnetite-rich bands which are separated by 60 m. Unlike magnetometry, the EM magnetite method is unaffected by remanent magnetism or magnetic latitude.

The EM magnetite mapping technique provides estimates of magnetite content which are usually correct within a factor of 2 when the magnetite is fairly uniformly distributed. EM magnetite maps can be generated when magnetic permeability is evident as negative in-phase responses on the data profiles.

Like magnetometry, the EM magnetite method maps only bedrock features, provided that the overburden is characterized by a general lack of magnetite. This contrasts with resistivity mapping which portrays the combined effect of bedrock and overburden.

The Susceptibility Effect

When the host rock is conductive, the positive conductivity response will usually dominate the secondary field, and the susceptibility effect[6] will appear as a reduction in the in-phase, rather than as a negative value. The in-phase response will be lower than would be predicted by a model using zero susceptibility. At higher frequencies the in-phase conductivity response also gets larger, so a negative magnetite effect observed on the low frequency might not be observable on the higher frequencies, over the same body. The susceptibility effect is most obvious over discrete magnetite-rich zones, but also occurs over uniform geology such as a homogeneous half-space.

High magnetic susceptibility will affect the calculated apparent resistivity, if only conductivity is considered. Standard apparent resistivity algorithms use a homogeneous half-space model, with zero susceptibility. For these algorithms, the reduced in-phase response will, in most cases, make the apparent resistivity higher than it should be. It is important to note that there is nothing wrong with the data, nor is there anything wrong with the processing algorithms. The apparent

---

[6] Magnetic susceptibility and permeability are two measures of the same physical property. Permeability is generally given as relative permeability, μ_r, which is the permeability of the substance divided by the permeability of free space ($4 \pi \times 10^{-7}$). Magnetic susceptibility k is related to permeability by $k=\mu^r-1$. Susceptibility is a unitless measurement, and is usually reported in units of 10^{-6}. The typical range of susceptibilities is –1 for quartz, 130 for pyrite, and up to 5×10^5 for magnetite, in 10^{-6} units (Telford et al, 1986).

difference results from the fact that the simple geological model used in processing does not match the complex geology.

Measuring and Correcting the Magnetite Effect

Theoretically, it is possible to calculate (forward model) the combined effect of electrical conductivity and magnetic susceptibility on an EM response in all environments. The difficulty lies, however, in separating out the susceptibility effect from other geological effects when deriving resistivity and susceptibility from EM data.

Over a homogeneous half-space, there is a precise relationship between in-phase, quadrature, and altitude. These are often resolved as phase angle, amplitude, and altitude. Within a reasonable range, any two of these three parameters can be used to calculate the half space resistivity. If the rock has a positive magnetic susceptibility, the in-phase component will be reduced and this departure can be recognized by comparison to the other parameters.

The algorithm used to calculate apparent susceptibility and apparent resistivity from HEM data, uses a homogeneous half-space geological model. Non half-space geology, such as horizontal layers or dipping sources, can also distort the perfect half-space relationship of the three data parameters. While it may be possible to use more complex models to calculate both rock parameters, this procedure becomes very complex and time-consuming. For basic HEM data processing, it is most practical to stick to the simplest geological model.

Magnetite reversals (reversed in-phase anomalies) have been used for many years to calculate an “FeO” or magnetite response from HEM data (Fraser, 1981). However, this technique could only be applied to data where the in-phase was observed to be negative, which happens when susceptibility is high and conductivity is low.

Applying Susceptibility Corrections

Resistivity calculations done with susceptibility correction may change the apparent resistivity. High-susceptibility conductors, that were previously masked by the

susceptibility effect in standard resistivity algorithms, may become evident. In this case the susceptibility corrected apparent resistivity is a better measure of the actual resistivity of the earth. However, other geological variations, such as a deep resistive layer, can also reduce the in-phase by the same amount. In this case, susceptibility correction would not be the best method. Different geological models can apply in different areas of the same data set. The effects of susceptibility, and other effects that can create a similar response, must be considered when selecting the resistivity algorithm.

Susceptibility from EM vs Magnetic Field Data

The response of the EM system to magnetite may not match that from a magnetometer survey. First, HEM-derived susceptibility is a rock property measurement, like resistivity. Magnetic data show the total magnetic field, a measure of the potential field, not the rock property. Secondly, the shape of an anomaly depends on the shape and direction of the source magnetic field. The electromagnetic field of HEM is much different in shape from the earth's magnetic field. Total field magnetic anomalies are different at different magnetic latitudes; HEM susceptibility anomalies have the same shape regardless of their location on the earth.

In far northern latitudes, where the magnetic field is nearly vertical, the total magnetic field measurement over a thin vertical dike is very similar in shape to the anomaly from the HEM-derived susceptibility (a sharp peak over the body). The same vertical dike at the magnetic equator would yield a negative magnetic anomaly, but the HEM susceptibility anomaly would show a positive susceptibility peak.

Effects of Permeability and Dielectric Permittivity

Resistivity algorithms that assume free-space magnetic permeability and dielectric permittivity, do not yield reliable values in highly magnetic or highly resistive areas. Both magnetic polarization and displacement currents cause a decrease in the in-phase component, often resulting in negative values that yield erroneously high apparent resistivities. The effects of magnetite occur at all frequencies, but are most evident at the lowest frequency. Conversely, the negative effects of dielectric permittivity are most evident at the higher frequencies, in resistive areas.

The table below shows the effects of varying permittivity over a resistive (10,000 ohm-m) half space, at frequencies of 56,000 Hz (DIGHEM^{V}) and 102,000 Hz (RESOLVE).

Apparent Resistivity Calculations

Effects of Permittivity on In-phase/Quadrature/Resistivity

Freq (Hz)	Coil	Sep (m)	Thres (ppm)	Alt (m)	In Phase	Quad Phase	App Res	App Depth (m)	Permittivity
56,000	CP	6.3	0.1	30	7.3	35.3	10118	-1.0	1 Air
56,000	CP	6.3	0.1	30	3.6	36.6	19838	-13.2	5 Quartz
56,000	CP	6.3	0.1	30	-1.1	38.3	81832	-25.7	10 Epidote
56,000	CP	6.3	0.1	30	-10.4	42.3	76620	-25.8	20 Granite
56,000	CP	6.3	0.1	30	-19.7	46.9	71550	-26.0	30 Diabase
56,000	CP	6.3	0.1	30	-28.7	52.0	66787	-26.1	40 Gabbro
102,000	CP	7.86	0.1	30	32.5	117.2	9409	-0.3	1 Air
102,000	CP	7.86	0.1	30	11.7	127.2	25956	-16.8	5 Quartz
102,000	CP	7.86	0.1	30	-14.0	141.6	97064	-26.5	10 Epidote
102,000	CP	7.86	0.1	30	-62.9	176.0	83995	-26.8	20 Granite
102,000	CP	7.86	0.1	30	-107.5	215.8	73320	-27.0	30 Diabase
102,000	CP	7.86	0.1	30	-147.1	259.2	64875	-27.2	40 Gabbro

Methods have been developed (Huang and Fraser, 2000, 2001) to correct apparent resistivities for the effects of permittivity and permeability. The corrected resistivities yield more credible values than if the effects of permittivity and permeability are disregarded.

Recognition of Culture

Cultural responses include all EM anomalies caused by man-made metallic objects. Such anomalies may be caused by inductive coupling or current gathering. The concern of the interpreter is to recognize when an EM response is due to culture. Points of consideration used by the interpreter, when coaxial and coplanar coil-pairs are operated at a common frequency, are as follows:

1. Channels CXPL and CPPL monitor 60 Hz radiation. An anomaly on these channels shows that the conductor is radiating power. Such an indication is normally a guarantee that the

conductor is cultural. However, care must be taken to ensure that the conductor is not a geologic body that strikes across a power line, carrying leakage currents.

2. A flight that crosses a "line" (e.g., fence, telephone line, etc.) yields a centre-peaked coaxial anomaly and an m-shaped coplanar anomaly.[7] When the flight crosses the cultural line at a high angle of intersection, the amplitude ratio of coaxial/coplanar response is 2. Such an EM anomaly can only be caused by a line. The geologic body that yields anomalies most closely resembling a line is the vertically dipping thin dike. Such a body, however, yields an amplitude ratio of 1 rather than 2. Consequently, an m-shaped coplanar anomaly with a CXI/CPI amplitude ratio of 2 is virtually a guarantee that the source is a cultural line.

3. A flight that crosses a sphere or horizontal disk yields centre-peaked coaxial and coplanar anomalies with a CXI/CPI amplitude ratio (i.e., coaxial/coplanar) of 1/8. In the absence of geologic bodies of this geometry, the most likely conductor is a metal roof or small fenced yard.[8] Anomalies of this type are virtually certain to be cultural if they occur in an area of culture.

4. A flight that crosses a horizontal rectangular body or wide ribbon yields an m-shaped coaxial anomaly and a centre-peaked coplanar anomaly. In the absence of geologic bodies of this geometry, the most likely conductor is a large fenced area.[5] Anomalies of this type are virtually certain to be cultural if they occur in an area of culture.

5. EM anomalies that coincide with culture, as seen on the camera film or video display, are usually caused by culture. However, care is taken with such coincidences because a geologic conductor could occur beneath a fence, for example. In this example, the fence would be expected to yield an m-shaped coplanar anomaly as in case #2 above. If, instead, a centre-peaked coplanar anomaly occurred, there would be concern that a thick geologic conductor coincided with the cultural line.

---

[7] See Figure C-1 presented earlier.

[8] It is a characteristic of EM that geometrically similar anomalies are obtained from: (1) a planar conductor, and (2) a wire which forms a loop having dimensions identical to the perimeter of the equivalent planar conductor.

6. The above description of anomaly shapes is valid when the culture is not conductively coupled to the environment. In this case, the anomalies arise from inductive coupling to the EM transmitter. However, when the environment is quite conductive (e.g., less than 100 ohm-m at 900 Hz), the cultural conductor may be conductively coupled to the environment. In this latter case, the anomaly shapes tend to be governed by current gathering. Current gathering can completely distort the anomaly shapes, thereby complicating the identification of cultural anomalies. In such circumstances, the interpreter can only rely on the radiation channels and on the camera film or video records.

Magnetic Responses

The measured total magnetic field provides information on the magnetic properties of the earth materials in the survey area. The information can be used to locate magnetic bodies of direct interest for exploration, and for structural and lithological mapping.

The total magnetic field response reflects the abundance of magnetic material in the source. Magnetite is the most common magnetic mineral. Other minerals such as ilmenite, pyrrhotite, franklinite, chromite, hematite, arsenopyrite, limonite and pyrite are also magnetic, but to a lesser extent than magnetite on average.

In some geological environments, an EM anomaly with magnetic correlation has a greater likelihood of being produced by sulphides than one which is non-magnetic. However, sulphide ore bodies may be non-magnetic (e.g., the Kidd Creek deposit near Timmins, Canada) as well as magnetic (e.g., the Mattabi deposit near Sturgeon Lake, Canada).

Iron ore deposits will be anomalously magnetic in comparison to surrounding rock due to the concentration of iron minerals such as magnetite, ilmenite and hematite.

Changes in magnetic susceptibility often allow rock units to be differentiated based on the total field magnetic response. Geophysical classifications may differ from geological classifications if various magnetite levels exist within one general geological classification. Geometric considerations of the

source such as shape, dip and depth, inclination of the earth's field and remanent magnetization will complicate such an analysis.

In general, mafic lithologies contain more magnetite and are therefore more magnetic than many sediments which tend to be weakly magnetic. Metamorphism and alteration can also increase or decrease the magnetization of a rock unit.

Textural differences on a total field magnetic contour, colour or shadow map due to the frequency of activity of the magnetic parameter resulting from inhomogeneities in the distribution of magnetite within the rock, may define certain lithologies. For example, near surface volcanics may display highly complex contour patterns with little line-to-line correlation.

Rock units may be differentiated based on the plan shapes of their total field magnetic responses. Mafic intrusive plugs can appear as isolated "bulls-eye" anomalies. Granitic intrusives appear as sub-circular zones, and may have contrasting rings due to contact metamorphism. Generally, granitic terrain will lack a pronounced strike direction, although granite gneiss may display strike.

Linear north-south units are theoretically not well-defined on total field magnetic maps in equatorial regions due to the low inclination of the earth's magnetic field. However, most stratigraphic units will have variations in composition along strike that will cause the units to appear as a series of alternating magnetic highs and lows.

Faults and shear zones may be characterized by alteration that causes destruction of magnetite (e.g., weathering) that produces a contrast with surrounding rock. Structural breaks may be filled by magnetite-rich, fracture filling material as is the case with diabase dikes, or by non-magnetic felsic material.

Faulting can also be identified by patterns in the magnetic total field contours or colours. Faults and dikes tend to appear as lineaments and often have strike lengths of several kilometres. Offsets in narrow, magnetic, stratigraphic trends also delineate structure. Sharp contrasts in magnetic lithologies may arise due to large displacements along strike-slip or dip-slip faults.

APPENDIX D

FLIGHT LOGS

SYSTEM ____ FLIGHT LOG JOB # 03069

FLIGHT: 03
DATE: 12/10/03
OPERATOR: DB
FLIGHT TIME:
TOTAL KMS:
VIDEO (ON) OFF
SPHERICS YES NO
TURBULENCE YES NO

SPECTROMETER ON / OFF	
System Calibrated On:	Cs / K / Th
Stabilized On	K / Th
Full Source Check	Yes / No
Cosmic flight for This Survey	No (not yet) / Yes

TEMP. START: _____ TEMP. END: _____
PRECIPITATION: _____ POST PROCESS: _____

Line	Dir	Start Fid	End Fid	Kms	**DATA ALERT**
10290	W	225	590	12.6	Start Time:
10280	E	625	945	12.7	
10270	W	1090	435		
10260	E	1460	1845		
10250	W	1895	2290		
10240	E	2315	2710		
10230	W	2865	3185		
10220	E	3210	3595		
10210	W	3535	3895		
10200	E	3870	4160		
10190	W	4360	4665		
10180	E	4685	5000		
10170	W	5030	5350		
10160	E	5375	5690		
10150	W	5900	6365		
10140	E	6390	6835		
10130	W	6865	7345		
					End Time: End Fid:

Ref. Position _____ N
_____ W
_____ M
Reference GPS _____
Mobile GPS 211103.737

Basemag: _____
EM Levels: _____

SYSTEM ___ FLIGHT LOG JOB # 03069

FLIGHT: 004
DATE: Dec 16, 2003
OPERATOR: DB
FLIGHT TIME:
TOTAL KMS:
VIDEO (ON) OFF
SPHERICS YES NO
TURBULENCE YES NO

SPECTROMETER ON / OFF	
System Calibrated On:	Cs / K / Th
Stabilized On	K / Th
Full Source Check	Yes / No
Cosmic flight for This Survey	No (not yet) / Yes

TEMP. START: _____ TEMP. END: _____
PRECIPITATION: _____ POST PROCESS: _____

	Line	Dir	Start Fid	End Fid	Kms	**DATA ALERT**
AC Q	10120	W	415		17.5	Start Time:
	10110	E	510	1365		
	10100	W	1400	1850		
Q	10090	E	2470	2630		
	10080	W	2690	3225		
	10070	E	3240	3770		
Q	10060	W	3945	4420		
	10050	E	4440	4765		
	10040	W	4825	5055		
	10030	E	5075	5340		
Q	10020	W	5510	5765		
	10010	E	5790	6035		
Q Q	50060	S	~~6375~~	~~7010~~		Mag landed & adjusted
			6950	~~7240~~		6949 7008
	50050	N	~~7240~~	~~7460~~	7110	7040 7105
	50040	S	~~7440~~	~~7665~~		7140 7196
	50030	N	7237	7298		
	50020	S	7346	7399		
	50010	N	7436	~~7474~~	~~??~~	7500
Q						
						End Time: End Fid:

Ref. Position _____ N
_____ W
_____ M
Reference GPS _____
Mobile GPS 1107.728

Basemag: _____
EM Levels: _____
86 133 3826 5445
6165 6875 7535

SYSTEM ____ FLIGHT LOG JOB # 05069

FLIGHT: 05
DATE: Dec 11/03
OPERATOR: DB
FLIGHT TIME:
TOTAL KMS:
VIDEO (ON) OFF
SPHERICS YES NO
TURBULENCE YES NO

SPECTROMETER ON / OFF	
System Calibrated On:	Cs / K / Th
Stabilized On	K / Th
Full Source Check	Yes / No
Cosmic flight for This Survey	No (not yet) / Yes

TEMP. START: _____ TEMP. END: _____
PRECIPITATION: _____ POST PROCESS: _____

Line	Dir	Start Fid	End Fid	Kms	**DATA ALERT**
10380	W	675	1020		Start Time:
10390	E	1065	1560		
10310	W	1595	1940		
10320	E	1965	2295		
10330	W	2455	2765		
10340	E	2790			
10350	W	3125	3440		
10360	E	3460	3775		
10370	W	3950	4260		
30010	E	4410	4670		
30020	W	4705	4945		
30030	E	4965	5200		
30040	W	5360	5640		
30050	E	5665	5940		
30060	W	5970	6235		
30070	E	6260			
30080	W	6710	6970		
30090	E	6995	7270		
30100	W	7300	7555		
30110	E	7580	7840		
					End Time: End Fid:

Ref. Position _____ N
_____ W
_____ M
Reference GPS _____
Mobile GPS 1207.736

Basemag: _____
EM Levels: _____
560 2415
3890 5310 6640 7940

SYSTEM ____ FLIGHT LOG JOB # 03069

FLIGHT: 06
DATE: Dec 13/03
OPERATOR: DB
FLIGHT TIME:
TOTAL KMS:
VIDEO (ON) OFF
SPHERICS YES NO TEMP. START: TEMP. END:
TURBULENCE YES NO PRECIPITATION: POST PROCESS:

SPECTROMETER ON / OFF	
System Calibrated On:	Cs / K / Th
Stabilized On	K / Th
Full Source Check	Yes / No
Cosmic flight for This Survey	No (not yet) / Yes

Line	Dir	Start Fid	End Fid	Kms	**DATA ALERT**
AC Q 30280	W	585	790		Start Time:
30310	E	805	985		
30360	W	1020	1195		
30350	E	1210	1385		
30340	W	1415	1685		
30330	E	1630	1810		
Q 30320	W	2020	2195		
30310	E	2220	2390		
30300	W	2425			
30290	E	2620	2790		
30280	W	2825	2995		
30270	E	~~3010~~	3190		
30260	W	3220	3425		
30250	E	3455	3650		
AC Q 30240	W	4000			
30230	E	4210	4390		
30220	W	4425	4635		
30210	E	4685	4920		
30200	W	4950	5192		
30190	E	5225	5460		
Q 30180	W	5670	5925		
30170	E	5965	6195		
30160	W	6230	6485		
30150	E	6505	6745		
Q 30140	W	6930	7180		
30130	E	7205	7450		
30120	W	7480	7735		
Q					
					End Time: End Fid:

Ref. Position N
W
M
Reference GPS
Mobile GPS 1408.105

Basemag:
EM Levels: 265 1930 3709 3950
5590 6863 7805

SYSTEM ____ FLIGHT LOG JOB #03069

FLIGHT: 07
DATE: Dec 14/03
OPERATOR: DB
FLIGHT TIME:
TOTAL KMS:
VIDEO (ON) OFF
SPHERICS YES NO
TURBULENCE YES NO

SPECTROMETER ON / OFF	
System Calibrated On:	Cs / K / Th
Stabilized On	K / Th
Full Source Check	Yes / No
Cosmic flight for This Survey	No (not yet) / Yes

TEMP. START: _____ TEMP. END: _____
PRECIPITATION: _____ POST PROCESS: _____

	Line	Dir	Start Fid	End Fid	Kms	**DATA ALERT**
Ic Q	10020	S	515	1015		Start Time:
		N	1160	1550		East Tie line
AC Q	WestLine	S	2030	2325		
	EastLine	N	2395	2605		
AC Q	10390	W	3470	3765		
	10400	E	3795	4070		
	10410	W	4095	4390		
	10420	E	4415	4680		
Q	10430	W	4920	5195		
	10440	E	5265	5485		
	10450	W	5510	5750		
	10460	E	5770	6005		
Q	10470	W	6185	6450		
	10480	E	6480	6735		
	10490	W	6755	6995		
	10500	E	7015	7240		
	10510	W	7275	7505		
Q	10570	E	7660	7895		
Q	10580	W	7920	8155		
						End Time: End Fid:

Ref. Position _____ N
_____ W
_____ M
Reference GPS _____
Mobile GPS 121500.749

Basemag: _____
EM Levels: 762 1679 1964 2716
3397 4812 6134 7612
8235

SYSTEM ____ FLIGHT LOG JOB #03069

FLIGHT: 08
DATE: Dec 14/03
OPERATOR: DB
FLIGHT TIME:
TOTAL KMS:
VIDEO (ON) OFF
SPHERICS YES NO
TURBULENCE (YES) NO

SPECTROMETER ON / OFF	
System Calibrated On:	Cs / K / Th
Stabilized On	K / Th
Full Source Check	Yes / No
Cosmic flight for This Survey	No (not yet) / Yes

TEMP. START: _____ TEMP. END: _____
PRECIPITATION: _____ POST PROCESS: _____

	Line	Dir	Start Fid	End Fid	Kms	**DATA ALERT**
K Q	10590	E	275	490		Start Time:
	10600	W	520	760		
	10610	E	775	995		
	10620	W	1035	1275		
Q	10630	E	1520	1730		
	10640	W	1770	2000		
	10650	E	2045	2285		
	10660	W	2310	2505		
	10670	E	2525	2700		
Q	10680	W	2865	3075		
	10690	E	3100	3295		
	10700	W	3320	35		
	10710	E	3520	3795		
	10720	W	3850	4070		
	10730	E	~~4040~~	4285		4130
Q	10740	W	4450	4630		
	10750	E	4655	4835		
	10760	W	4920	5090		
	10770	E	5120	5275		
	10780	W	5300	5495		
	10790	E	5520	5675		
Q	10800	W	5860	6040		
	10810	E	6065	6220		
	10820	W	6240	6415		
	10830	E	6440	6590		
	10840	W	6610	6790		
	10850	E	6820	6960		
	10860	W	7030	7145		
	10870	E	7165	7345		
	10880	W	7285	7365		
	10890	E	7385	7450		
Q						
						End Time: End Fid:

Ref. Position _____ N
_____ W
_____ M
Reference GPS _____
Mobile GPS 1215 Ø41.T2Ø

Basemag: _____
EM Levels: _____
210 1395 2815
4385 5805 7495

SYSTEM ___ FLIGHT LOG JOB # 0369

FLIGHT: 09
DATE: Dec 14/03
OPERATOR: DB
FLIGHT TIME:
TOTAL KMS:
VIDEO (ON) OFF
SPHERICS YES NO
TURBULENCE (YES) NO

SPECTROMETER ON / OFF	
System Calibrated On:	Cs / K / Th
Stabilized On	K / Th
Full Source Check	Yes / No
Cosmic flight for This Survey	No (not yet) / Yes

TEMP. START: _____ TEMP. END: _____
PRECIPITATION: _____ POST PROCESS: _____

Line	Dir	Start Fid	End Fid	Kms	**DATA ALERT**
LT test Cable		19	27		Start Time:
2000ft		60	70		
3000ft		107	117		
4000ft		165	175		
C Q 10520	W	515	760		
10530	E	776	980		
10540	W	1010	1240		
10550	E	1260	1465		
10560	W	1490	1735		
Q					
					End Time: End Fid:

Ref. Position _____ N
_____ W
_____ M
Reference GPS _____
Mobile GPS 1215073730

Basemag: _____
EM Levels: _____
_____
450 1315

Appendix E – Tests and Calibrations

Altimeter Test – Performed December 14, 2003 over landing site at Camp Stanley

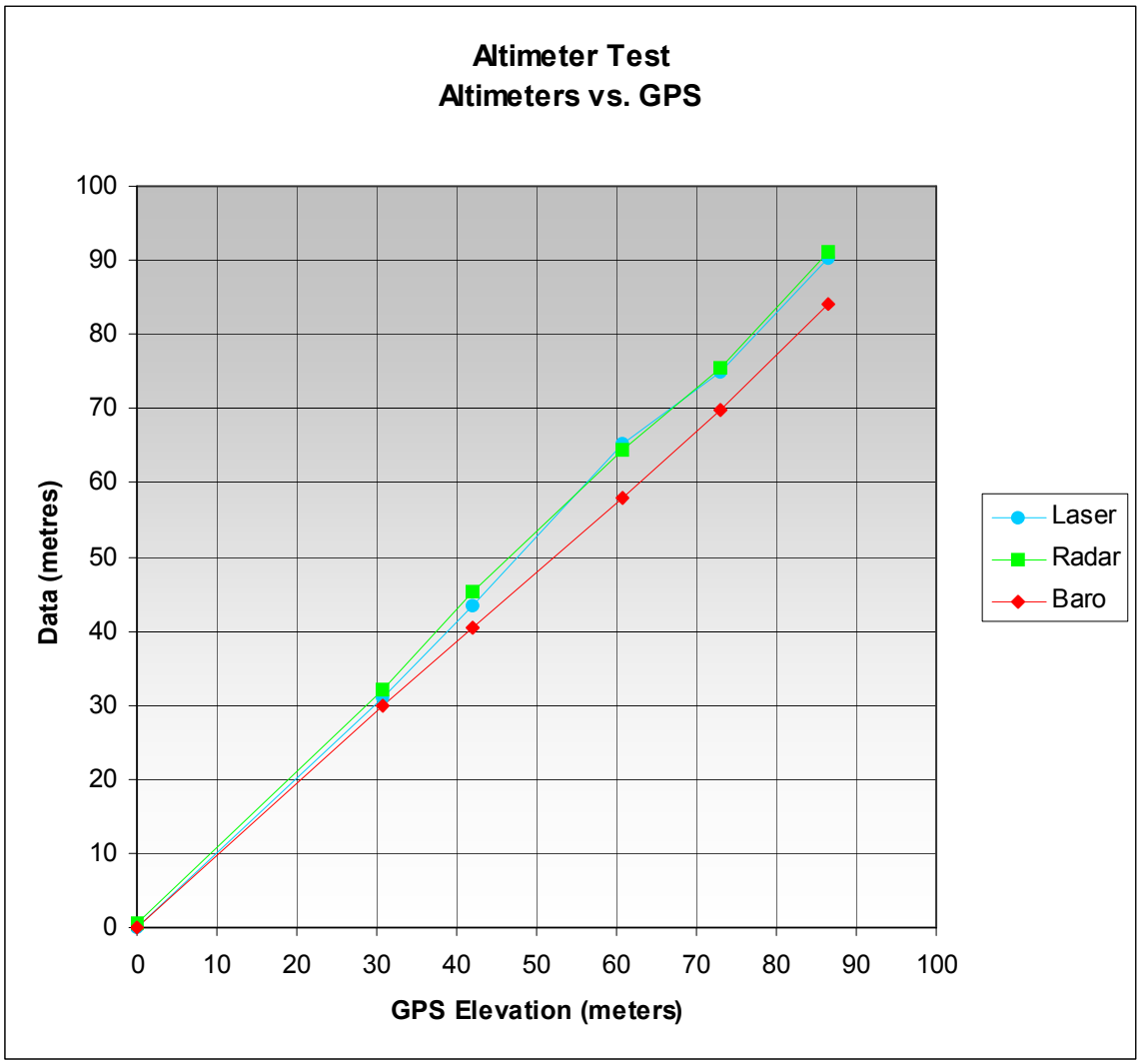

-barometric and GPS data zeroed at the first point to match radar and laser data

-radar data has 27.7 metres removed from raw to represent bird altitude.

EM Calibrations

CALIBRATION OF THE DIGHEM DIGITAL (DSP) SYSTEM

The calibration method used in the digital Dighem^{V} has been developed as a significant improvement over the practices described by Fitterman (1998), which practices were originally developed through experimentation and consultation between Fugro and the United States Geological Survey. The problems defined by Fitterman, including jig calibration and conductive ground response, are obviated by calibration at high altitude using internal, rigidly mounted, automatically triggered and measured calibration coils.

Calibration of the system during the survey will use the Fugro AutoCal™ automatic, internal calibration process. At the beginning and end of each flight, and at intervals during the flight, the system will be flown up to high altitude to remove it from any "ground effect" (response from the earth). Any remaining signal from the receiver coils (base level) will be measured as the zero level, and removed from the data collected until the time of the next calibration. Following the zero level setting, internal calibration coils, for which the response phase and amplitude have been determined at the factory, are automatically triggered – one for each frequency. The on-time of the coils is sufficient to determine an accurate response through any ambient noise. The receiver response to each calibration coil "event" is compared to the expected response (from the factory calibration) for both phase angle and amplitude, and the applied phase and gain corrections adjusted to bring the data to the correct value.

In addition, the output of the transmitter coils are continuously monitored during the survey, and the applied gains adjusted to correct for any change in transmitter output (due to heating, etc.)

Because the internal calibration coils are calibrated at the factory (on a resistive halfspace) ground calibrations using external calibration coils on-site are not necessary for system calibration. A check calibration may be carried out on-site to ensure all systems are working correctly. All system calibrations will be carried out in the air, at sufficient altitude that there will be no measurable response from the ground.

The internal calibration coils are rigidly positioned and mounted in the system relative to the transmitter and receiver coils. In addition, when the internal calibration coils are calibrated at the factory, a rigid jig is employed to ensure accurate response from the external coils.

Using real time Fast Fourier Transforms and the calibration procedures outlined above, the data will be processed in real time from measured total field at a high sampling rate to in-phase and quadrature values at 10 samples per second.

Greg Hodges, Chief Geophysicist 01/04/09

References:

Fitterman, D.V., (1998). Sources of calibration errors in helicopter EM data. Exploration Geophysics 29, 65-70.

External Calibration Results

Dec 11, 2003 Start calibration. On site at Camp Stanley

FREQUENCY	CHANNEL	INTERNAL		EXTERNAL		PHASE
		MEASURED	TARGET	MEASURED	TARGET	(degrees)
400	L400I	195.0	196.2	188.0	200.4	-1.0
	L400Q	194.0	196.2	194.0	200.4	
1500	L1K5I	176.0	178.4	215.0	204.2	-3.0
	L1K5Q	176.0	178.4	191.0	204.2	
3300	L1K7I	103.0	104.4	104.0	99.9	-0.8
	L1K7Q	104.0	104.4	101.0	99.9	
6200	L6K2I	829.0	823.5	196.0	207.5	-0.1
	L6K2Q	831.0	823.5	201.0	207.5	
25000	L25KI	509.0	504.6	174.0	192.5	0.1
	L25KQ	505.0	504.6	173.0	192.5	
100000	L100I	480.0	460.6	208.0	178.8	-2.0
	L100Q	480.0	460.6	210.0	178.8	

Dec 20, 2003 End calibration. At Fugro's calibrations site, Mountsburg, Ontario

FREQUENCY	CHANNEL	INTERNAL		EXTERNAL		PHASE
		MEASURED	TARGET	MEASURED	TARGET	
400	L400I	196.0	196.2	180.0	200.4	-1.9
	L400Q	196.0	196.2	195.0	200.4	
1500	L1K5I	180.0	178.4	192.0	204.2	-3.5
	L1K5Q	180.0	178.4	198.0	204.2	
3300	L1K7I	103.0	104.4	111.0	99.9	-1.2
	L1K7Q	103.0	104.4	110.0	99.9	
6200	L6K2I	824.0	823.5	185.0	207.5	-1.8
	L6K2Q	823.0	823.5	185.0	207.5	
25000	L25KI	505.0	504.6	192.0	192.5	-1.4
	L25KQ	505.0	504.6	182.0	192.5	
100000	L100I	475.0	460.6	193.0	178.8	-2.2
	L100Q	480.0	460.6	194.0	178.8	

-phase calculated from inverse TAN of quad deflection/inphase deflection. Variations attributed to temperature changes from the different times and locations of the calibrations.

Appendix F - Processing Log

Total Magnetic Field data

A fourth difference was calculated from the raw total magnetic intensity data (TMI). The raw TMI was examined in profile form along with the fourth difference. Spikes and duplicate points were manually defaulted and interpolated with an Akima spline. None of the defaulted areas exceeded one second in length. The diurnal variations recorded by the base station were edited for any cultural contamination and filtered to remove high-frequency noise. This diurnal magnetic data was then subtracted from the despiked TMI to provide a first order diurnal correction. An average base value of 48517 nT was added back to the diurnal corrected airborne total magnetic field records. The diurnal removed magnetic field data were then gridded and compared to a grid of the despiked magnetic data to ensure that the data quality was improved by diurnal removal.

The lag in the magnetic data was determined and applied to the survey data. A vertical gradient was calculated from the lagged magnetic data and examined for evidence of lag and leveling problems. The lag of –0.5 seconds seemed appropriate for the survey data and few leveling errors were noted. The IGRF was calculated using the latest coefficient set for a date of 2003/12/12 with the altitude taken from the differentially corrected height above the WGS84 spheroid. The calculated IGRF was removed from the magnetic data prior to any tie line leveling. Tie line leveling corrections were calculated and applied with additional manual corrections to a few of the survey lines. Vertical gradient grids were calculated from the magnetic grids after each leveling correction. These grids were shadowed and examined to determine the success of the manual correction. To remove any short wavelength residual line-to-line discrepancies in the total magnetic field, a microleveling technique was used to remove errors of less than 2.5 nT striking parallel to the line direction. This microleveled channel was used to produce the final residual magnetic field grid. The IGRF was recalculated using the latest coefficient set for a date of 2003/12/12 with the altitude set at 425.0 m. The new IGRF correction was added to the final residual magnetic field to produce the final total magnetic field, IGRF corrected.

Electromagnetic and Resistivity data

Base level corrections were picked off of the analogue rolls from the high altitude backgrounds. These level picks were applied to the raw EM data which were then loaded into the Geosoft database. An 11-point median filter followed by an 11-point Hanning filter was applied to the raw base leveled data. (13-point filters were used on the CP400 Hz EM data). Apparent resistivity and depth calculations were done on the filtered, base leveled EM data using Fugro's proprietary resistivity algorithm. All in-phase, quadrature and resistivity channels were gridded and examined, and manual leveling corrections and phase adjustments were applied as required. The resistivity calculation and gridding was repeated until no further corrections were required. Additional algorithms were run on the data to determine the centroid depths, differential resistivity and differential depths. Sengpiel-type and differential resistivity depth sections were generated to double check the resistivity leveling.

Two sets of grids were generated. The 100 metre spaced detail area was windowed out of the block and gridded with 20 metre cells (1/5 of the line spacing). The remaining area flown at 200-metre spacing was gridded using 40 metre cells. A grid function was run on the 40 metre grids to reduce the cell size to 20 metres and the two grids were merged together, averaging the grid values in a 2 cell overlap. The merged grids were then filtered for final presentation using the following rectangular Hanning filter values:

RES115K	3x3
RES25K	3x3
RES6200	5x5
RES1500	11x11
RES400	19x19

The filtered grids were written back to the database as database channels with a "_filt" suffix. The digital grid archive also contains unfiltered and filtered grids.

Grids for area B3 were gridded with 10 metre cells and were filtered in a similar manner as above. B3 filtered and unfiltered grids are included in the digital grid archive, filtered and unfiltered channels are included in the digital data archive.

Appendix G - GLOSSARY OF AIRBORNE GEOPHYSICAL TERMS

Note: The definitions given in this glossary refer to the common terminology as used in airborne geophysics.

altitude attenuation: the absorption of gamma rays by the atmosphere between the earth and the detector. The number of gamma rays detected by a system decreases as the altitude increases.

apparent- : the ***physical parameters*** of the earth measured by a geophysical system are normally expressed as apparent, as in "apparent ***resistivity***". This means that the measurement is limited by assumptions made about the geology in calculating the response measured by the geophysical system. Apparent resistivity calculated with ***HEM***, for example, generally assumes that the earth is a ***homogeneous half-space*** – not layered.

amplitude: The strength of the total electromagnetic field. In ***frequency domain*** it is most often the sum of the squares of ***in-phase*** and ***quadrature*** components. In multi-component electromagnetic surveys it is generally the sum of the squares of all three directional components.

analytic signal: The total amplitude of all the directions of magnetic ***gradient***. Calculated as the sum of the squares.

anisotropy: Having different ***physical parameters*** in different directions. This can be caused by layering or fabric in the geology. Note that a unit can be anisotropic, but still **homogeneous**.

anomaly: A localized change in the geophysical data characteristic of a discrete source, such as a conductive or magnetic body. Something locally different from the **background**.

B-field: In time-domain **electromagnetic** surveys, the magnetic field component of the (electromagnetic) **field**. This can be measured directly, although more commonly it is calculated by integrating the time rate of change of the magnetic field **dB/dt**, as measured with a receiver coil.

background: The "normal" response in the geophysical data – that response observed over most of the survey area. **Anomalies** are usually measured relative to the background. In airborne gamma-ray

spectrometric surveys the term defines the **cosmic**, radon, and aircraft responses in the absence of a signal from the ground.

base-level: The measured values in a geophysical system in the absence of any outside signal. All geophysical data are measured relative to the system base level.

base frequency: The frequency of the pulse repetition for a ***time-domain electromagnetic*** system. Measured between subsequent positive pulses.

bird: A common name for the pod towed beneath or behind an aircraft, carrying the geophysical sensor array.

calibration coil: A wire coil of known size and dipole moment, which is used to generate a field of known ***amplitude*** and ***phase*** in the receiver, for system calibration. Calibration coils can be external, or internal to the system. Internal coils may be called Q-coils.

coaxial coils: **[CX]** Coaxial coils are in the vertical plane, with their axes horizontal and collinear in the flight direction. These are most sensitive to vertical conductive objects in the ground, such as thin, steeply dipping conductors perpendicular to the flight direction. Coaxial coils generally give the sharpest anomalies over localized conductors. (See also ***coplanar coils***)

coil: A multi-turn wire loop used to transmit or detect electromagnetic fields. Time varying ***electromagnetic*** fields through a coil induce a voltage proportional to the strength of the field and the rate of change over time.

compensation: Correction of airborne geophysical data for the changing effect of the aircraft. This process is generally used to correct data in ***fixed-wing time-domain electromagnetic*** surveys (where the transmitter is on the aircraft and the receiver is moving), and magnetic surveys (where the sensor is on the aircraft, turning in the earth's magnetic field.

component: In ***frequency domain electromagnetic*** surveys this is one of the two **phase** measurements – ***in-phase or quadrature***. In "multi-component" electromagnetic surveys it is also used to define the measurement in one geometric direction (vertical, horizontal in-line and horizontal transverse – the Z, X and Y components).

Compton scattering: gamma ray photons will bounce off the nuclei of atoms they pass through (earth and atmosphere), reducing their energy and then being detected by ***radiometric*** sensors at lower energy levels. See also ***stripping***.

conductance: See ***conductivity thickness***

conductivity: [σ] The facility with which the earth or a geological formation conducts electricity. Conductivity is usually measured in milli-Siemens per metre (mS/m). It is the reciprocal of ***resistivity***.

conductivity-depth imaging: see ***conductivity-depth transform***.

conductivity-depth transform: A process for converting electromagnetic measurements to an approximation of the conductivity distribution vertically in the earth, assuming a ***layered earth***. (Macnae and Lamontagne, 1987; Wolfgram and Karlik, 1995)

conductivity thickness: [σ**t**] The product of the ***conductivity***, and thickness of a large, tabular body. (It is also called the "conductivity-thickness product") In electromagnetic geophysics, the response of a thin plate-like conductor is proportional to the conductivity multiplied by thickness. For example a 10 metre thickness of 20 Siemens/m mineralization will be equivalent to 5 metres of 40 S/m; both have 200 S conductivity thickness. Sometimes referred to as conductance.

conductor: Used to describe anything in the ground more conductive than the surrounding geology. Conductors are most often clays or graphite, or hopefully some type of mineralization, but may also be man-made objects, such as fences or pipelines.

coplanar coils: **[CP]** The coplanar coils lie in the horizontal plane with their axes vertical, and parallel. These coils are most sensitive to massive conductive bodies, horizontal layers, and the ***halfspace***.

cosmic ray: High energy sub-atomic particles from outer space that collide with the earth's atmosphere to produce a shower of gamma rays (and other particles) at high energies.

counts (per second): The number of ***gamma-rays*** detected by a gamma-ray ***spectrometer.*** The rate depends on the geology, but also on the size and sensitivity of the detector.

culture: A term commonly used to denote any man-made object that creates a geophysical anomaly. Includes, but not limited to, power lines, pipelines, fences, and buildings.

current gathering: The tendency of electrical currents in the ground to channel into a conductive formation. This is particularly noticeable at higher frequencies or early time channels when the formation is long and parallel to the direction of current flow. This tends to enhance anomalies relative to inductive currents (see also ***induction***). Also known as current channelling.

current channelling: See current gathering.

daughter products: The radioactive natural sources of gamma-rays decay from the original element (commonly potassium, uranium, and thorium) to one or more lower-energy elements. Some of these lower energy elements are also radioactive and decay further. ***Gamma-ray spectrometry*** surveys may measure the gamma rays given off by the original element or by the decay of the daughter products.

dB/dt: As the ***secondary electromagnetic field*** changes with time, the magnetic field [**B**] component induces a voltage in the receiving ***coil***, which is proportional to the rate of change of the magnetic field over time.

decay: In ***time-domain electromagnetic*** theory, the weakening over time of the ***eddy currents*** in the ground, and hence the ***secondary field*** after the ***primary field*** electromagnetic pulse is turned off. In ***gamma-ray spectrometry***, the radioactive breakdown of an element, generally potassium, uranium, thorium, or one of their ***daughter*** products.

decay series: In ***gamma-ray spectrometry***, a series of progressively lower energy ***daughter products*** produced by the radioactive breakdown of uranium or thorium.

decay constant: see time constant.

depth of exploration: The maximum depth at which the geophysical system can detect the target. The depth of exploration depends very strongly on the type and size of the target, the contrast of the target with the surrounding geology, the homogeneity of the surrounding geology, and the type of geophysical system. One measure of the maximum depth of exploration for an electromagnetic system is the depth at which it can detect the strongest conductive target – generally a highly conductive horizontal layer.

differential resistivity: A process of transforming ***apparent resistivity*** to an approximation of layer resistivity at each depth. The method uses multi-frequency HEM data and approximates the effect of shallow layer ***conductance*** determined from higher frequencies to estimate the deeper conductivities (Huang and Fraser, 1996)

dipole moment: [NIA] For a transmitter, the product of the area of a ***coil***, the number of turns of wire, and the current flowing in the coil. At a distance significantly larger than the size of the coil, the magnetic field from a coil will be the same if the dipole moment product is the same. For a receiver coil, this is the product of the area and the number of turns. The sensitivity to a magnetic field (assuming the source is far away) will be the same if the dipole moment is the same.

diurnal: The daily variation in a natural field, normally used to describe the natural fluctuations (over hours and days) of the earth's magnetic field.

dielectric permittivity: **[ε]** The capacity of a material to store electrical charge, this is most often measured as the relative permittivity [ε_r], or ratio of the material dielectric to that of free space. The effect of high permittivity may be seen in HEM data at high frequencies over highly resistive geology as a reduced or negative ***in-phase***, and higher ***quadrature*** data.

drift: Long-time variations in the base-level or calibration of an instrument.

eddy currents: The electrical currents induced in the ground, or other conductors, by a time-varying ***electromagnetic field*** (usually the ***primary field***). Eddy currents are also induced in the aircraft's metal frame and skin; a source of ***noise*** in EM surveys.

electromagnetic: **[EM]** Comprised of a time-varying electrical and magnetic field. Radio waves are common electromagnetic fields. In geophysics, an electromagnetic system is one which transmits a time-varying ***primary field*** to induce ***eddy currents*** in the ground, and then measures the ***secondary field*** emitted by those eddy currents.

energy window: A broad spectrum of ***gamma-ray*** energies measured by a spectrometric survey. The energy of each gamma-ray is measured and divided up into numerous discrete energy levels, called windows.

equivalent (thorium or uranium): The amount of radioelement calculated to be present, based on the gamma-rays measured from a **daughter** element. This assumes that the ***decay series*** is in equilibrium – progressing normally.

fiducial, or fid: Timing mark on a survey record. Originally these were timing marks on a profile or film; now the term is generally used to describe 1-second interval timing records in digital data, and on maps or profiles.

fixed-wing: Aircraft with wings, as opposed to "rotary wing" helicopters.

footprint: This is a measure of the area of sensitivity under the aircraft of an airborne geophysical system. The footprint of an ***electromagnetic*** system is dependent on the altitude of the system, the orientation of the transmitter and receiver and the separation between the receiver and transmitter, and the conductivity of the ground. The footprint of a ***gamma-ray spectrometer*** depends mostly on the altitude. For all geophysical systems, the footprint also depends on the strength of the contrasting ***anomaly***.

frequency domain: An ***electromagnetic*** system which transmits a ***primary field*** that oscillates smoothly over time (sinusoidal), inducing a similarly varying electrical current in the ground. These systems generally measure the changes in the ***amplitude*** and ***phase*** of the ***secondary field*** from the ground at different frequencies by measuring the **in-phase** and **quadrature** phase components. See also ***time-domain***.

full-stream data: Data collected and recorded continuously at the highest possible sampling rate. Normal data are stacked (see ***stacking***) over some time interval before recording.

gamma-ray: A very high-energy photon, emitted from the nucleus of an atom as it undergoes a change in energy levels.

gamma-ray spectrometry: Measurement of the number and energy of natural (and sometimes man-made) gamma-rays across a range of photon energies.

gradient: In magnetic surveys, the gradient is the change of the magnetic field over a distance, either vertically or horizontally in either of two directions. Gradient data is often measured, or calculated from the total magnetic field data because it changes more quickly over distance than

the ***total magnetic field***, and so may provide a more precise measure of the location of a source. See also ***analytic signal***.

ground effect: The response from the earth. A common calibration procedure in many geophysical surveys is to fly to altitude high enough to be beyond any measurable response from the ground, and there establish ***base levels*** or ***backgrounds***.

half-space: A mathematical model used to describe the earth – as infinite in width, length, and depth below the surface. The most common halfspace models are ***homogeneous*** and ***layered earth***.

heading error: A slight change in the magnetic field measured when flying in opposite directions.

HEM: Helicopter ElectroMagnetic, This designation is most commonly used to helicopter-borne, ***frequency-domain*** electromagnetic systems. At present, the transmitter and receivers are normally mounted in a ***bird*** carried on a sling line beneath the helicopter.

herringbone pattern: a pattern created in geophysical data by an asymmetric system, where the **anomaly** may be extended to either side of the source, in the direction of flight. Appears like fish bones, or like the teeth of a comb, extending either side of centre, each tooth an alternate flight line.

homogeneous: This is a geological unit that has the same ***physical parameters*** throughout its volume. This unit will create the same response to an HEM system anywhere, and the HEM system will measure the same apparent ***resistivity*** anywhere. The response may change with system direction (see ***anisotropy***).

in-phase: the component of the measured ***secondary field*** that has the same phase as the transmitter and the ***primary field***. The in-phase component is stronger than the ***quadrature*** phase over relatively higher ***conductivity***.

induction: Any time-varying electromagnetic field will induce (cause) electrical currents to flow in any object with non-zero ***conductivity***. (see ***eddy currents***)

infinite: In geophysical terms, an "infinite' dimension is one much greater than the ***footprint*** of the system, so that the system does not detect changes at the edges of the object.

International Geomagnetic Reference Field: **[IGRF]** An approximation of the smooth magnetic field of the earth, in the absence of variations due to local geology. Once the IGRF is subtracted from the measured magnetic total field data, any remaining variations are assumed to be due to local geology. The IGRF also predicts the slow changes of the field up to five years in the future.

inversion, or **inverse modeling**: A process of converting geophysical data to an earth model, which compares theoretical models of the response of the earth to the data measured, and refines the model until the response closely fits the measured data (Huang and Palacky, 1991)

layered earth: A common geophysical model which assumes that the earth is horizontally layered – the ***physical parameters*** are constant to ***infinite*** distance horizontally, but change vertically.

magnetic permeability: **[μ]** This is defined as the ratio of magnetic induction to the inducing magnetic field. The relative magnetic permeability [μ_r] is often quoted, which is the ratio of the rock permeability to the permeability of free space. In geology and geophysics, the ***magnetic susceptibility*** is more commonly used to describe rocks.

magnetic susceptibility: **[k]** A measure of the degree to which a body is magnetized. In SI units this is related to relative ***magnetic permeability*** by $k=\mu_r-1$, and is a dimensionless unit. For most geological material, susceptibility is influenced primarily by the percentage of magnetite. It is most often quoted in units of 10^{-6}. In HEM data this is most often apparent as a negative ***in-phase*** component over high susceptibility, high ***resistivity*** geology such as diabase dikes.

noise: That part of a geophysical measurement that the user does not want. Typically this includes electronic interference from the system, the atmosphere (***sferics***), and man-made sources. This can be a subjective judgment, as it may include the response from geology other than the target of interest. Commonly the term is used to refer to high frequency (short period) interference. See also ***drift***.

Occam's inversion: an ***inversion*** process that matches the measured ***electromagnetic*** data to a theoretical model of many, thin layers with constant thickness and varying resistivity (Constable et al, 1987).

off-time: In a ***time-domain electromagnetic*** survey, the time after the end of the ***primary field pulse***, and before the start of the next pulse.

on-time: In a ***time-domain electromagnetic*** survey, the time during the ***primary field pulse***.

phase: The angular difference in time between a measured sinusoidal electromagnetic field and a reference – normally the primary field. The phase is calculated from $\tan^{-1}$(***in-phase / quadrature***).

physical parameters: These are the characteristics of a geological unit. For electromagnetic surveys, the important parameters for electromagnetic surveys are ***conductivity, magnetic permeability*** (or ***susceptibility***) and ***dielectric permittivity***; for magnetic surveys the parameter is magnetic susceptibility, and for gamma ray spectrometric surveys it is the concentration of the major radioactive elements: potassium, uranium, and thorium.

permittivity: see ***dielectric permittivity***.

permeability: see ***magnetic permeability***.

primary field: the EM field emitted by a transmitter. This field induces ***eddy currents*** in (energizes) the conductors in the ground, which then create their own ***secondary*** **fields**.

pulse: In time-domain EM surveys, the short period of intense ***primary*** field transmission. Most measurements (the ***off-time***) are measured after the pulse.

quadrature: that component of the measured ***secondary field*** that is phase-shifted 90° from the ***primary field***. The quadrature component tends to be stronger than the ***in-phase*** over relatively weaker ***conductivity***.

Q-coils: see ***calibration coil***.

radiometric: Commonly used to refer to ***gamma ray*** spectrometry.

radon: A radioactive daughter product of uranium and thorium, radon is a gas which can leak into the atmosphere, adding to the non-geological background of a gamma-ray spectrometric survey.

resistivity: **[ρ]** The strength with which the earth or a geological formation resists the flow of electricity, typically the flow induced by the ***primary field*** of the electromagnetic transmitter. Normally expressed in ohm-metres, it is the reciprocal of ***conductivity***.

resistivity-depth transforms: similar to ***conductivity depth transforms***, but the calculated ***conductivity*** has been converted to ***resistivity***.

resistivity section: an approximate vertical section of the resistivity of the layers in the earth. The resistivities can be derived from the ***apparent resistivity***, the ***differential resistivities***, ***resistivity-depth transforms***, or ***inversions***.

secondary field: The field created by conductors in the ground, as a result of electrical currents induced by the ***primary field*** from the ***electromagnetic*** transmitter. Airborne ***electromagnetic*** systems are designed to create, and measure a secondary field.

Sengpiel section: a ***resistivity section*** derived using the ***apparent resistivity*** and an approximation of the depth of maximum sensitivity for each frequency.

sferic: Lightning, or the ***electromagnetic*** signal from lightning, it is an abbreviation of "atmospheric discharge". These appear to magnetic and electromagnetic sensors as sharp "spikes" in the data. Under some conditions lightning storms can be detected from hundreds of kilometres away. (see ***noise***)

signal: That component of a measurement that the user wants to see – the response from the targets, from the earth, etc. (See also ***noise***)

skin depth: A measure of the depth of penetration of an electromagnetic field into a material. It is defined as the depth at which the primary field decreases to 1/e of the field at the surface. It is calculated by approximately 503 x √(resistivity/frequency). Note that depth of penetration is greater at higher ***resistivity*** and/or lower ***frequency***.

spectrometry: Measurement across a range of energies, where ***amplitude*** and energy are defined for each measurement. In gamma-ray spectrometry, the number of gamma rays are measured for each energy ***window***, to define the ***spectrum***.

spectrum: In ***gamma ray spectrometry***, the continuous range of energy over which gamma rays are measured. In ***time-domain electromagnetic*** surveys, the spectrum is the energy of the **pulse** distributed across an equivalent, continuous range of frequencies.

spheric: see ***sferic***.

stacking: Summing repeat measurements over time to enhance the repeating ***signal***, and minimize the random ***noise***.

stripping: Estimation and correction for the gamma ray photons of higher and lower energy that are observed in a particular ***energy window***. See also ***Compton scattering***.

susceptibility: See ***magnetic susceptibility***.

tau: [τ] Often used as a name for the ***time constant***.

TDEM: ***time domain electromagnetic***.

thin sheet: A standard model for electromagnetic geophysical theory. It is usually defined as thin, flat-lying, and ***infinite*** in both horizontal directions. (see also ***vertical plate***)

tie-line: A survey line flown across most of the ***traverse lines***, generally perpendicular to them, to assist in measuring ***drift*** and ***diurnal*** variation. In the short time required to fly a tie-line it is assumed that the drift and/or diurnal will be minimal, or at least changing at a constant rate.

time constant: The time required for an ***electromagnetic*** field to decay to a value of 1/e of the original value. In ***time-domain*** electromagnetic data, the time constant is proportional to the size and ***conductance*** of a tabular conductive body. Also called the decay constant.

Time channel: In ***time-domain electromagnetic*** surveys the decaying ***secondary field*** is measured over a period of time, and the divided up into a series of consecutive discrete measurements over that time.

time-domain: ***Electromagnetic*** system which transmits a pulsed, or stepped ***electromagnetic*** field. These systems induce an electrical current (***eddy current***) in the ground that persists after the ***primary***

field is turned off, and measure the change over time of the ***secondary field*** created as the currents ***decay***. See also ***frequency-domain***.

total energy envelope: The sum of the squares of the three ***components*** of the ***time-domain electromagnetic secondary field***. Equivalent to the ***amplitude*** of the secondary field.

transient: Time-varying. Usually used to describe a very short period pulse of ***electromagnetic*** field.

traverse line: A normal geophysical survey line. Normally parallel traverse lines are flown across the property in spacing of 50 m to 500 m, and generally perpendicular to the target geology.

vertical plate: A standard model for electromagnetic geophysical theory. It is usually defined as thin, and ***infinite*** in horizontal dimension and depth extent. (see also ***thin shee***t)

waveform: The shape of the ***electromagnetic pulse*** from a ***time-domain*** electromagnetic transmitter.

window: A discrete portion of a ***gamma-ray spectrum*** or ***time-domain electromagnetic decay***. The continuous energy spectrum or ***full-stream*** data are grouped into windows to reduce the number of samples, and reduce ***noise***.

Version 1.1, March 10, 2003
Greg Hodges,
Chief Geophysicist
Fugro Airborne Surveys, Toronto

Common Symbols and Acronyms

k	Magnetic susceptibility
ε	Dielectric permittivity
μ, μ_r	Magnetic permeability, apparent permeability
ρ, ρ_a	Resistivity, apparent resistivity
σ,σ_a	Conductivity, apparent conductivity
σt	Conductivity thickness
τ	Tau, or time constant

Ω.m Ohm-metres, units of resistivity

AGS Airborne gamma ray spectrometry.

CDT Conductivity-depth transform, conductivity-depth imaging (Macnae and Lamontagne, 1987; Wolfgram and Karlik, 1995)

CPI, CPQ Coplanar in-phase, quadrature

CPS Counts per second

CTP Conductivity thickness product

CXI, CXQ Coaxial, in-phase, quadrature

fT femtoteslas, normal unit for measurement of B-Field

EM Electromagnetic

keV kilo electron volts – a measure of gamma-ray energy

MeV mega electron volts – a measure of gamma-ray energy 1MeV = 1000keV

NIA dipole moment: turns x current x Area

nT nano-Tesla, a measure of the strength of a magnetic field

ppm parts per million – a measure of secondary field or noise relative to the primary.

pT/s picoTeslas per second: Units of decay of secondary field, dB/dt

S Siemens – a unit of conductance

x: the horizontal component of an EM field parallel to the direction of flight.

y: the horizontal component of an EM field perpendicular to the direction of flight.

z: the vertical component of an EM field.

References:

Constable, S.C., Parker, R.L., And Constable, C.G., 1987, Occam's inversion: a practical algorithm for generating smooth models from electromagnetic sounding data: Geophysics, 52, 289-300

Huang, H. and Fraser, D.C, 1996. The differential parameter method for muiltifrequency airborne resistivity mapping. Geophysics, 55, 1327-1337

Huang, H. and Palacky, G.J., 1991, Damped least-squares inversion of time-domain airborne EM data based on singular value decomposition: Geophysical Prospecting, v.39, 827-844

Macnae, J. and Lamontagne, Y., 1987, Imaging quasi-layered conductive structures by simple processing of transient electromagnetic data: Geophysics, v52, 4, 545-554.

Sengpiel, K-P. 1988, Approximate inversion of airborne EM data from a multi-layered ground. Geophysical Prospecting, 36, 446-459

Wolfgram, P. and Karlik, G., 1995, Conductivity-depth transform of GEOTEM data: Exploration Geophysics, 26, 179-185.

Yin, C. and Fraser, D.C., 2002, The effect of the electrical anisotropy on the responses of helicopter-borne frequency domain electromagnetic systems, Submitted to *Geophysical Prospecting*